Molecular Therapy
Nucleic Acids
Original Article

Metabolism pathway-based subtyping in endometrial cancer: An integrated study by multi-omics analysis and machine learning algorithms

Xiaodie Liu,[1,4] Wenhui Wang,[2] Xiaolei Zhang,[3] Jing Liang,[2] Dingqing Feng,[2] Yuebo Li,[1] Ming Xue,[1] and Bin Ling[1]

[1]Department of Obstetrics and Gynecology, China-Japan Friendship Hospital (Institute of Clinical Medical Sciences), Chinese Academy of Medical Sciences & Peking Union Medical College, Beijing 100029, China; [2]Department of Obstetrics and Gynecology, China-Japan Friendship Hospital, Beijing 100029, China; [3]Department of Obstetrics and Gynecology, Qilu Hospital of Shandong University, No. 107 Wenhua West Road, Jinan, Shandong 250012, China; [4]Department of Obstetrics and Gynecology, Shandong Provincial Hospital, Jinan 250000, China

Endometrial cancer (EC), the second most common malignancy in the female reproductive system, has garnered increasing attention for its genomic heterogeneity, but understanding of its metabolic characteristics is still poor. We explored metabolic dysfunctions in EC through a comprehensive multi-omics analysis (RNA-seq datasets from The Cancer Genome Atlas [TCGA], Cancer Cell Line Encyclopedia [CCLE], and GEO datasets; the Clinical Proteomic Tumor Analysis Consortium [CPTAC] proteomics; CCLE metabolomics) to develop useful molecular targets for precision therapy. Unsupervised consensus clustering was performed to categorize EC patients into three metabolism-pathway-based subgroups (MPSs). These MPS subgroups had distinct clinical prognoses, transcriptomic and genomic alterations, immune microenvironment landscape, and unique patterns of chemotherapy sensitivity. Moreover, the MPS2 subgroup had a better response to immunotherapy. Finally, three machine learning algorithms (LASSO, random forest, and stepwise multivariate Cox regression) were used for developing a prognostic metagene signature based on metabolic molecules. Thus, a 13-hub gene-based classifier was constructed to predict patients' MPS subtypes, offering a more accessible and practical approach. This metabolism-based classification system can enhance prognostic predictions and guide clinical strategies for immunotherapy and metabolism-targeted therapy in EC.

INTRODUCTION

Metabolism reprogramming has been regarded as a hallmark of cancer cells, which fosters tumor initiation and progression.[1] This phenomenon, known as aerobic glycolysis or the Warburg effect, allows cancer cells to preferentially use glucose to produce lactate even in the presence of oxygen, providing a rapid energy supply for proliferation and contributing to anabolic pathways for amino acids, lipids, and nucleotide synthesis.[2–5] The tricarboxylic acid (TCA) cycle further generates essential metabolites such as aspartate and citrate, facilitating tumor growth and metastasis for most cancer cells.[6–9] In recent years, extensive research has delved into multiple metabolic pathways in cancer with the understanding of nutrient competition.[10] In addition to supporting anabolism, tumor metabolites can act as signaling molecules with tumorigenic effects and remodel the tumor immune microenvironment to evade immune surveillance.[11–13]

Intricate interactions between gene mutations, involving oncogenic or tumor suppressor genes, and downstream signaling pathways (e.g., phosphatidylinositol 3-kinase-AKT-mammalian target of rapamycin complex 1 [PI3K-AKT-mTORC1] and MYC), orchestrate the dysregulation of metabolic enzyme expression, promoting cancer cell survival.[14–17] Moreover, the extrinsic tumor microenvironment (TME), characterized by nutrient constraints, low oxygen levels, and an acidic milieu, drives cancer cells to adapt their metabolic pathways. Consequently, the interplay between genetic alterations and external environmental stresses contributes to tumor metabolic heterogeneity within the same tissue.[18–20] Targeting metabolism enzymes with drugs holds great promise because it not only offers the potential to eliminate tumor cells but it also remodels the TME, thereby enhancing tumor immunity.[21,22] However, the low specificities of metabolic inhibitors hamper their effectiveness, causing normal tissue toxicity and acquiring resistance.[23]

Endometrial cancer (EC) is heterogeneous cancer, histologically classified as endometrioid and non-endometrioid types (serous, clear cell, undifferentiated, mesonephric, mesonephric-like, squamous, mucinous intestinal type, and mixed carcinomas and carcinosarcoma), and categorized into The Cancer Genome Atlas (TCGA) four molecular subgroups according to molecular profile, polymerase

Received 6 September 2023; accepted 14 February 2024;
https://doi.org/10.1016/j.omtn.2024.102155.

Correspondence: Dingqing Feng, Department of Obstetrics and Gynecology, China-Japan Friendship Hospital (Institute of Clinical Medical Sciences), Chinese Academy of Medical Sciences & Peking Union Medical College, Beijing 100029, China.
E-mail: fengdingqing@zryhyy.com.cn
Correspondence: Bin Ling, Department of Obstetrics and Gynecology, China-Japan Friendship Hospital (Institute of Clinical Medical Sciences), Chinese Academy of Medical Sciences & Peking Union Medical College, Beijing 100029, China.
E-mail: lingbin@zryhyy.com.cn

ε ultramutated, microsatellite instability hypermutated (MSI), copy-number low (CN-L), and copy-number high (CN-H).[24] It ranks as the second most common gynecologic cancer among women, with its incidence on the rise due to factors such as obesity and an aging population.[25,26] Surgery (minimally invasive surgical staging and sentinel lymph node biopsy) is the mainstream therapy for EC. Advances in our understanding of the molecular biology of EC have paved the way for targeted chemotherapy and immunotherapy strategies, especially in adjuvant, advanced, and recurrent disease settings and those desiring fertility-sparing treatment.[27–30] Several previous studies have pointed to metabolism dysregulation as an important risk factor for EC initiation and progression.[31,32] Other past studies have centered primarily on cell-level metabolism inhibitor therapies.[33] However, there remains a paucity of studies on understanding its impact on tumor biology, therapeutic outcomes, and clinical therapies, remaining an area that warrants further exploration.

In this study, we comprehensively analyzed the overall metabolism dysregulation of EC using transcriptomics and proteomics data. Based on 84 different metabolic pathways, we identified metabolism pathway-related molecular subgroups that reflected distinct clinical features, genomic alterations, metabolic profiles, TME immune infiltration, immunotherapy response, and chemotherapy sensitivity. Furthermore, we developed a quantitative metabolism-based gene signature using machine learning algorithms to predict prognosis and guide precision therapy decisions in EC.

RESULTS

Transcriptomic and proteomic profiles revealed metabolism reprogramming of EC

To investigate whether metabolism reprogramming occurred in EC, we first conducted principal-component analysis (PCA) comparing normal (para- and normal endometrium) with tumor tissues and found distinct metabolic transcriptional profiles, whereas different histological types and grades of EC had relatively similar expression patterns in both TCGA and GSE17025 cohorts (Figures 1A, 1B, S1A, and S1B). Patients with endometrial hyperplasia without atypia adjacent to EC tissue also shared similar expression patterns of metabolic-related genes to paired tumor tissue in the GSE106191 cohort (Figure S1C). Consequently, gene set enrichment analysis (GSEA) analysis was further performed on the differentially expressed genes (DEGs) between EC and normal/precancerous tissue to reveal the significantly changed metabolic pathways. The dysregulated pathways appeared to encompass most metabolic processes, with a majority of them being upregulated in the EC tumor samples (Figures S1D–S1F). Within the top 10 upregulated pathways across all 3 datasets, a consistent activation was observed in both the glycolysis/gluconeogenesis and folate biosynthesis pathways (Figure 1C).

Subsequently, at the protein level, the Clinical Proteomic Tumor Analysis Consortium (CPTAC) EC proteome study analyzed 10,180 protein levels of 131 samples along with their corresponding biospecimen information. However, only 1,161 metabolism pathway-related proteins were investigated. Moreover, the PCA analysis confirmed that EC exhibited a distinct metabolic landscape compared to normal tissue based on the protein-level metabolic pathways (Figure 1D). Differential analysis on CPTAC transformed data (log2 (num + 10)) between EC and normal tissue revealed 120 DEGs with statistical significance ($p < 0.05$, log fold change [FC] >0.05) (Figure S1G). Similar to the above transcriptomic data (GSE17025 and TCGA EC cohorts), the oxidative phosphorylation and glycan biosynthesis pathways were found to be significantly activated in EC compared to normal tissue in the CPTAC cohort (Figures 1E, S1H, and S1I). These findings demonstrate the presence of metabolic reprogramming in samples of EC.

Metabolism pathway-based subtyping of EC

To reveal the metabolism heterogeneity of EC, we carried out consensus clustering and NbClust testing analysis on the gene set variation analysis (GSVA)-derived enrichment scores of 84 metabolic pathways and identified 3 as the optimal clustering number in the TCGA cohort. PCA also confirmed that 3 was the best number for clustering. Subsequently, a total of 548 patients were classified into 3 distinct metabolism pathway-based subgroup (MPS) clusters: MPS1 (35.9%), MPS2 (33.4%), and MPS3 (30.7%) (Figures 2A, 2B, S2A, and S2B). MPS1 exhibited a "hot" metabolic profile, encompassing nearly all metabolic categories. MPS2 demonstrated upregulation in specific lipid metabolism and amino acid metabolism pathways, including primary bile acid biosynthesis, steroid hormone biosynthesis, and linoleic acid metabolism, among others. In contrast, MPS3 displayed a relatively "cold" metabolic phenotype compared to the other two clusters (Figure 2C).

We further investigated the clinicopathological features among three metabolism-related subtypes. Kaplan-Meier (KM) survival analysis revealed that the MPS3 subtype had the worst overall survival (OS) (log rank test, $p < 0.05$) and disease-free survival (DFS) (log rank test, $p = 0.067$) compared with the other two subtypes (Figure 2D). Univariate Cox regression analysis confirmed that MPS3 had a worse OS (hazard ratio [HR] 2.22, 95% confidence interval [CI] 1.32–3.75, $p = 0.0026$) and DFS (HR 1.74, 95% CI 1.08–2.78, $p = 0.02$) about the MPS2 cluster. However, no significant differences in OS and DFS were observed between MPS1 and MPS2 ($p > 0.05$). The MPS3 cluster exhibited a higher proportion of EC patients with the serous histological type, grade 2–3, and stage III–IV compared to the other two clusters ($p < 0.001$) (Figure 2E). Patients in the MPS3 cluster tended to be older compared to those in the MPS1/2 clusters ($p = 0.082$) (Figure S2C). Comparison of the TCGA molecular subgroups[34] with the MPS clusters revealed that the MPS3 cluster was predominantly composed of the CN-H type, whereas the MPS2 cluster demonstrated a higher proportion of the CN-L type ($p < 0.001$) (Figure 2F; Table S3). Subgroup analysis revealed that the largest subset of EC (referred to as the nonspecific molecular profile [NSMP], also known as CN-L) exhibited heterogeneous metabolic profiles across MPS clusters. Importantly, within the MPS1 subgroup, NSMP patients demonstrated a tendency toward poor OS (Figures 2G and S2D). Similarly, among patients in the MSI or not-assigned groups with an intermediate prognosis, those falling within the MPS3 subgroup

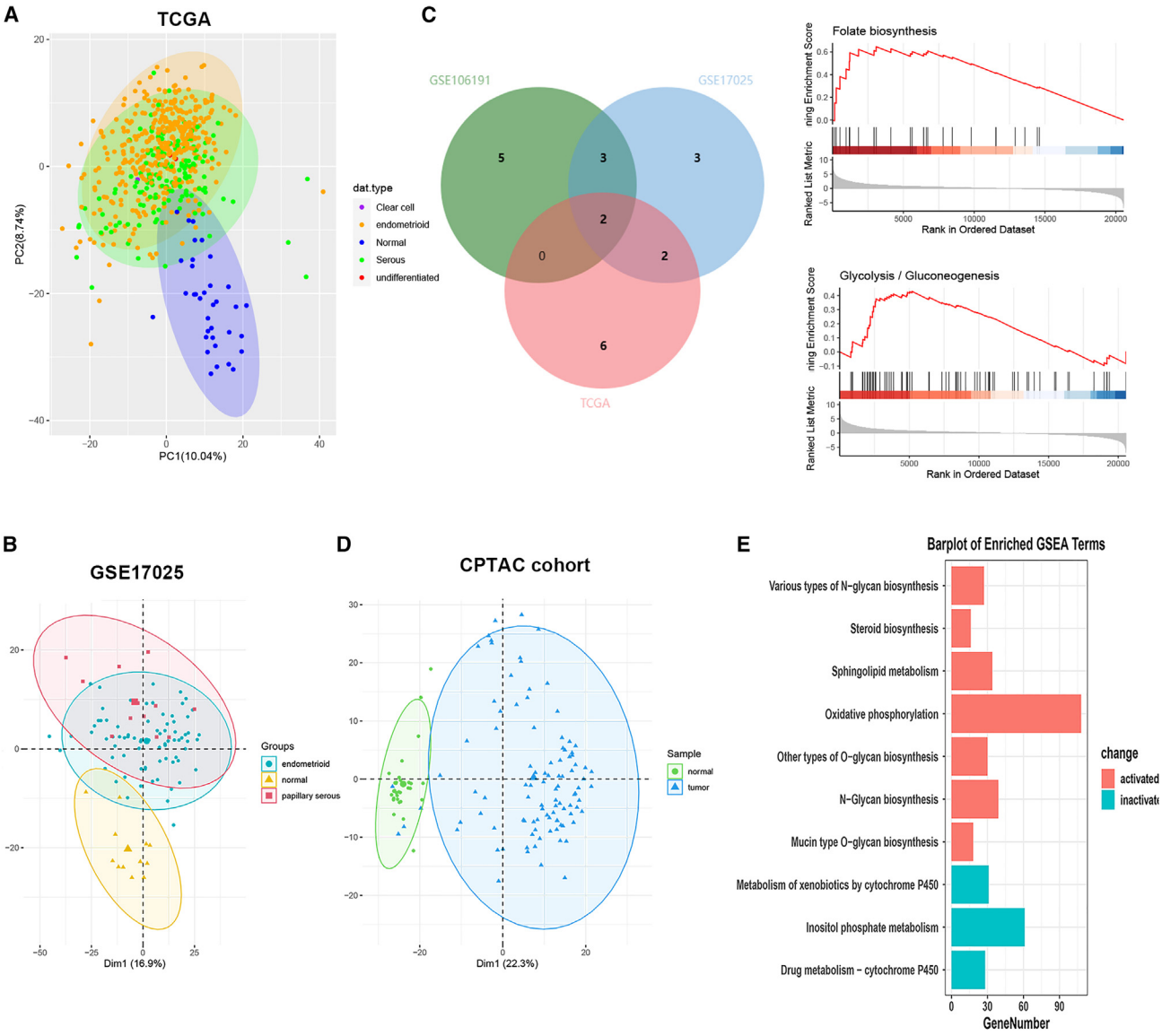

Figure 1. Transcriptomic and proteomic profiles revealed metabolism reprogramming of EC

(A and B) PCA plot of metabolic genes in the TCGA cohort (A) and GSE17025 (B). (C) Venn diagram illustrating the shared upregulated metabolic pathways among the TCGA, GSE106191, and GSE17025 cohorts (left); and representative GSEA plots showcasing glycolysis/gluconeogenesis and folate biosynthesis pathways in the TCGA cohort (right). (D) PCA plot of metabolic genes at the protein level in the CPTAC cohort. (E) Bar plots depicting GSEA on differentially expressed metabolic genes in the CPTAC EC cohort, comparing tumor samples to normal samples.

exhibited a shorter recurrence duration, although the difference did not reach statistical significance (Figure S2E). In summary, these findings underscore the intricate interplay between TCGA molecular subtypes and metabolic profiles, shedding light on the prognostic nuances within NSMP EC.

Transcriptomic profiling comparison among MPS subtypes

The heterogeneous metabolic phenotypes prompted us to explore the potential molecular characteristics of different MPS subgroups based on transcriptional profiling. We first identified significantly altered metabolism pathway-related genes of each MPS cluster by comparative analysis (Figure S3A; Table S4). Next, we determined whether these key metabolic enzyme expression levels were linked with the enrichment scores of metabolic pathways in different MPS clusters. GSEA analysis further uncovered metabolic heterogeneity among MPS clusters, and the enriched metabolic pathways in each subgroup were highly consistent with those identified through differential analysis based on GSVA scores (Figures S3B–S3D). The MPS1 subgroup displayed upregulation in pentose and glucuronate interconversions, arginine and proline metabolism, and glutathione

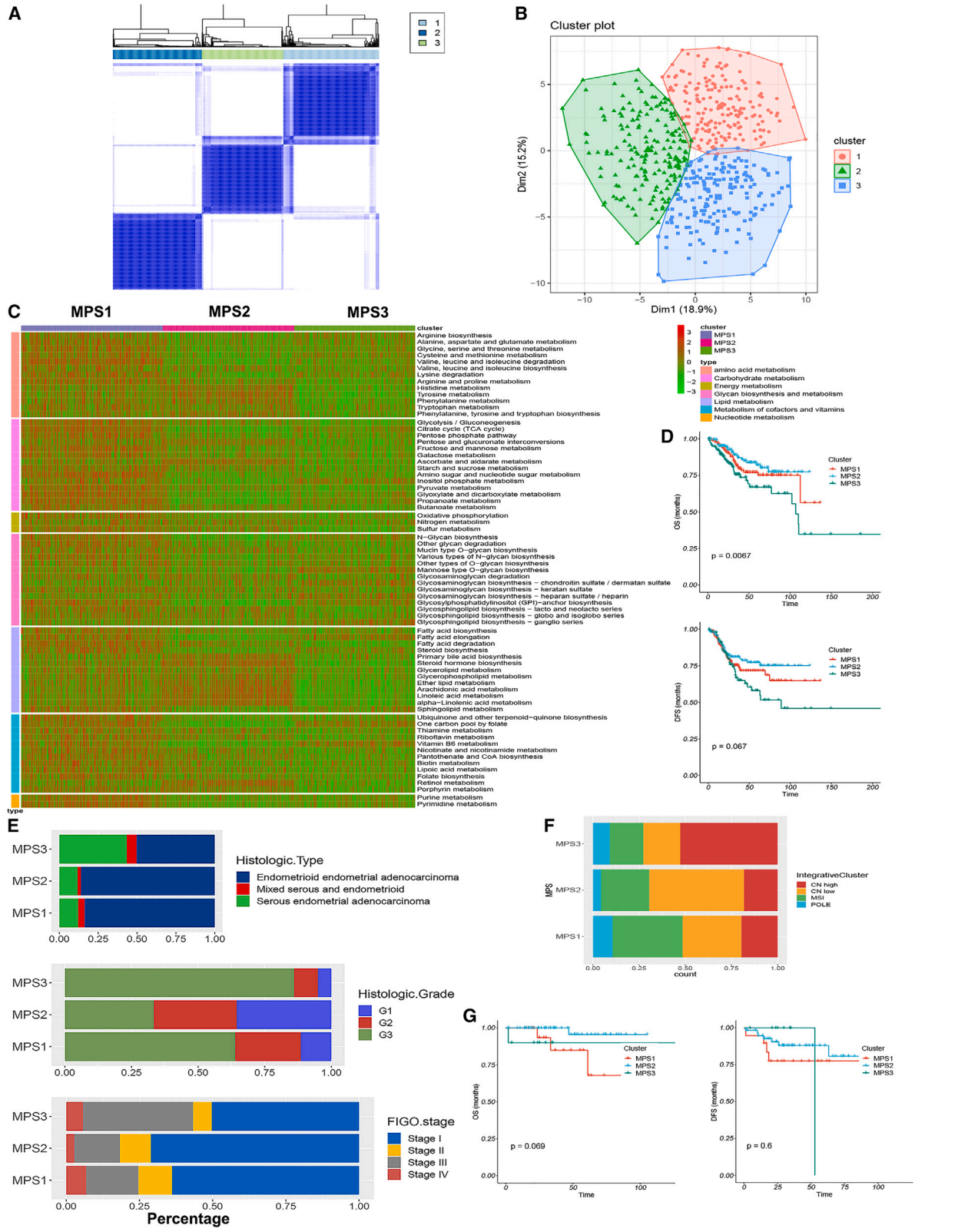

(legend on next page)

metabolism, featuring specific gene overexpression such as UDP glucuronosyltransferase family 1 member A6 (UGT1A6), nucleoside diphosphate kinase 2 (NME2), and aldo-keto reductase family 1 member B10 (AKR1B10). Tumors in MPS2 exhibited enrichment in α-linoleic acid metabolism, arachidonic acid metabolism, fatty acid degradation, and drug metabolism, with elevated expression of genes such as alcohol dehydrogenase 1B (ADH1B), phospholipase A2 group IIC (PLA2G2C), glutathione S-transferase alpha 3 (GSTA3), and cytochrome P450 family 2 subfamily B member 6 (CYP2B6). Conversely, fatty acid elongation was inactivated, as indicated by the lower expression of ELOVL family genes. In stark contrast, the MPS3 cluster demonstrated downregulation of retinol metabolism, steroid hormone biosynthesis, glycolysis/gluconeogenesis, unsaturated fatty acid, and pyruvate metabolism pathways, of which mRNA expression of alcohol dehydrogenase 4 (ADH4), phospholipase A2 group IIC (PLA2G2C), and cytochrome P450 monooxygenase (CYP) family genes was downregulated (Figures 3A–3C).

Delving into the intricate molecular landscape of EC, we intricately dissected the activation patterns of hallmark signaling pathways across the three distinct MPS subtypes. Pathways enrolled in the cell cycle, including MYC, E2F, G2M, and mitotic, were conspicuously activated in the MPS1 and MPS3 subgroups, whereas they were inactivated within the MPS2 cluster (Figures 3D and S4A). Tumor metabolic reprogramming has been previously reported to be closely associated with the epithelial-to-mesenchymal transition (EMT).[35] Intriguingly, the EMT scores and EMT-related gene expression, such as SRY-box transcription factor 9 (SOX9), twist family bHLH transcription factor 1 (TWIST1), forkhead box F1 (FOXF1), zinc finger E-box binding homeobox 1 (ZEB1), zinc finger E-box binding homeobox 2 (ZEB2), and GATA binding protein 6 (GATA6), were relatively lower in MPS1 than the other two clusters (Figures 3E and 3F). Following correlation analysis, amino acid metabolism pathways (e.g., glycine, serine, and threonine metabolism; cysteine and methionine metabolism; lysine degradation), carbohydrate metabolism pathways (including the TCA cycle, pentose phosphate pathway, glyoxylate and dicarboxylate metabolism), biosynthesis-related pathways (glycosylphosphatidylinositol biosynthesis, fatty acid elongation, and steroid synthesis), cofactors, and nucleotide metabolism were discerned. Notably, these pathways, integral to cell replication and proliferation, were identified. Furthermore, the glycosaminoglycan synthesis pathway was found to be linked to tumor EMT (Figure 3G). We thus amalgamated subtype-specific metabolic characteristics that significantly influence tumor behavior within the MPS subtypes, summarizing distinctive metabolic therapies (Table S5). MPS1 suggests targeting strategies involving inhibitors of glucose metabolism and amino acid metabolism. MPS3 suggests targeting nucleotide metabolism, specifically interrupting DNA synthesis. Meanwhile, MPS2 indicates potential benefits from exogenous α-linoleic acid treatment, as previous literature has indicated.[36] Targeting tumor cell metabolism presents a promising avenue for molecular interventions.[37]

Featured genomic alterations among MPS clusters in EC

Genomic alterations, such as tumor suppressor (e.g., von-Hippel Lindau) loss of function and oncogene gain of function (leading to PI3K/AKT/mTOR activity), are likely to result in cancer metabolic reprogramming.[18] We explored the top 10 mutated genes of each subgroup and found completely different mutation profiles among 3 MPS subgroups (Figures S5A–S5C). We then compared the mutation frequencies of 10 classical oncogenic pathways among the 3 MPS clusters.[38] The MPS1 subgroup showed significantly higher mutation frequencies in the PI3K, nuclear factor erythroid 2-related factor 2 (NRF2), transforming growth factor β (TGF-β), MYC, Hippo, and Notch pathways, whereas the MPS3 cluster was characterized by the highest mutation in the TP53 pathway. Notably, members in the PI3K pathway were highly mutated in the MPS1/2 cluster ($p < 0.05$) (Figure 4A). This observation positions MPS1 as a potential candidate for targeted therapies leveraging small-molecule inhibitors tailored to these specific pathways. When focusing on MPS subtype-specific metabolism-related mutated genes, we noticed that the MPS1 cluster has comparatively higher mutation frequencies among the PI3K members (phosphatase and tensin homolog [PTEN], 67.6%), and lysine degradation pathway members (lysine methyltransferase 2D, KMT2D, 39.6%; lysine methyltransferase 2C, KMT2C, 26.4%; lysine methyltransferase 2A, KMT2A, 21.4%; SET domain containing 2, histone lysine methyltransferase, SETD2, 7.47%; and nuclear receptor binding SET domain protein 1, NSD1, 25.3%) ($p < 0.05$) (Figure 4B; Table S6). KMT subfamily genes catalyze the various lysine methylation events decorating the core histone proteins, which induces epigenomic and metabolic reprogramming in multiple types of cancer.[39] For example, KMT2D regulates multiple glycolytic genes, thus conferring a therapeutic vulnerability to glycolytic inhibitors.[40] Consequently, we have gained profound insights into tumor metabolic heterogeneity by analyzing gene mutation profiles. This knowledge forms the basis for developing targeted therapeutics tailored to specific MPS subtypes.

In terms of somatic copy-number variation (CNV) differences, we also observed among three MPS clusters that MPS3 has a relatively higher CNV burden and chromosome instability level (Figures 4C and S5D). The amplification or deletion regions of each cluster are shown in Figures 4D–4F. MPS1 has a relatively high amplification frequency in 3:1q22 (50%), 2:1q21.3 (48%), 4:1q25.3 (46%), 5:1q32.1 (42%), and 24:8q24.21 (37%); MPS2 in 2:1q22 (44%), 1:1q21.3

Figure 2. Metabolism pathway-related stratification of EC

(A) EC patients were clustered into 3 subgroups based on GSVA scores of 84 metabolic pathways. (B) PCA on the metabolic pathways GSVA scores showed 3 distinct MPS subgroups in the TCGA cohort. (C) Heatmap of the normalized enrichment scores for 84 KEGG metabolic pathways among the TCGA EC MPS subgroups. (D) KM curves of OS (upper) and DFS (lower) among the 3 subtypes in the TCGA cohort. (E and F) Bar plots depicting the distribution of different histological types, grades, FIGO stages (E), and TCGA molecular subgroups (F) among the 3 MPS clusters. (G) Comparison of OS and DFS in NSMP patients among MPS subgroups.

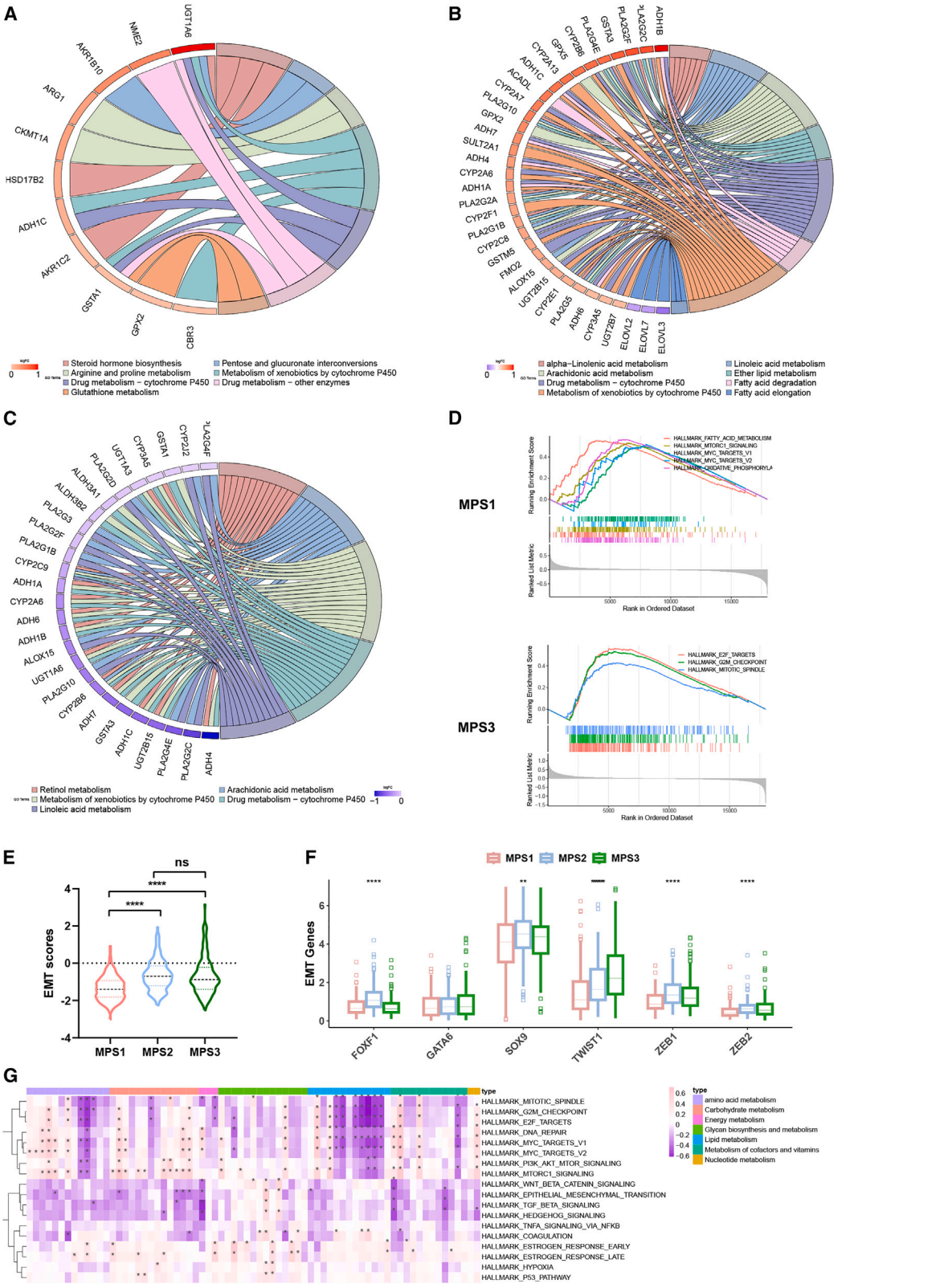

(legend on next page)

(44%), 20:10q22.2 (28%), 16:8q11.23 (27%), and 17:8q22.3 (27%); and MPS3 in 28:8q24.21 (59%), 6:1q22 (58%), 5:1q21.3 (56%), 13:3q26.2 (53%), and 25:8q11.23 (52%) (Figure S5E). Kyoto Encyclopedia of Genes and Genomes (KEGG) analysis revealed that genes with amplification were enriched in the nitrogen metabolism and glycosaminoglycan synthesis pathways in the MPS1 cluster; signaling pathways regulating the pluripotency of stem cells and cancer pathways in the MPS2 cluster, and ribosome, TGF-βsignaling, EGFR tyrosine kinase inhibitor resistance, and cholesterol metabolism in the MPS3 cluster ($p < 0.01$) (Figures 4G–4I). These results indicated that the amplification of the chromosomal region was comparatively consistent with the activation of metabolic pathways of ECs. Meanwhile, the higher chromosomal instability level explained worse DFS[41] and potential clinical benefits from poly (ADP-ribose) polymerase (PARP) inhibitors and Pt-containing therapy in the MPS3 subgroup.[42]

Distinct immune microenvironment infiltration and heterogeneous responses to immunotherapy among MPS subgroups

As previous literature has reported, various metabolic changes and epigenetic modifications have also been reported to play an important role in tumor progression by driving immune escape or hindering immune surveillance.[1,43,44] In our study, we observed an enriched presence of CD4 T cells, M0 macrophages, M2 macrophages, and regulatory T cells (Tregs) within the TME of EC (Figure S6A). Compared with the other clusters, MPS2 exhibited a notably elevated abundance of CD4 memory resting T cells and Tregs. In contrast, the levels of follicular helper T cells, M1 and M2 macrophages, activated mast cells, and neutrophils were comparatively lower ($p < 0.05$) (Figure 5A). As expected, the infiltration of lymphocytes showed a gradual decline from MPS2 to MPS3 and MPS1 clusters, with the highest levels of total macrophages and M2/M1 ratio observed in MPS1 ($p < 0.05$) (Figures S6B and S6C). We also observed a lower immune infiltration level in the MPS3 subgroup by the single-sample GSEA (ssGSEA) algorithm, and total immune cells exerting antitumor or protumor effects both increased in the MPS2 subgroup (Figures S6D and 5B). We could conclude that the metabolic heterogeneity of EC is closely associated with the occurrence of TME changes.

Although past studies have undeniably established the effectiveness of immunotherapy in EC, the responsiveness to this treatment varies considerably among individual patients.[45] Specifically, we explored whether different MPS subgroups showed varying sensitivity to immunotherapy since substantial differences in immune cell infiltration existed within each subgroup. The estimated immune scores and dysfunction scores of the MPS2 cluster were higher than the MPS3 cluster (Figures S6E and 5C). However, the Tumor Immune Dysfunction and Exclusion (TIDE) scores and exclusion scores were lower in the MPS1 cluster than in the other clusters ($p < 0.05$) (Figures 5D and 5E). The tumor mutation burden (TMB) level was also the highest in the MPS1 cluster, which indicated a better response to immunotherapy (Figure 5F). Previous literature confirmed that lymphocyte activation 3 (LAG3) expression in peripheral blood cells identified patients with poorer outcomes after immune checkpoint blockade.[46] Notably, elevated expression levels of interferon gamma receptor 1 (IFNGR1) and LAG3 were observed in the MPS3 subgroup, whereas the MPS2 cluster exhibited higher levels of cytotoxic T lymphocyte-associated protein 4 (CTLA4) and programmed cell death 1 (PDCD1) (Figure 5G). Undoubtedly, the predictive response rate was highest in the MPS2 subgroup according to the TIDE algorithm (Figure 5H). In conclusion, contrasting the two clusters, although the MPS2 cluster exhibited abundant immune cell infiltration, it concurrently presented indications of immune dysfunction. However, the MPS1 cluster, characterized by elevated TMB and lower TIDE scores, suggests a reduced likelihood of immune escape, accompanied by increased production of novel tumor antigens. Compared with the MPS3 subgroup, the other two subgroups may benefit from immunotherapy.

Metabolism pathway-based subtyping reflects unique chemotherapy sensitivity and metabolic profiles at the cellular level

In addition to conventional chemotherapy, we aimed to explore novel, highly effective molecular targeted drugs based on MPS subtypes to enhance precision therapeutic outcomes. Overall, the top 10 drugs with the lowest predicted area under the curve (AUC) values in the total TCGA cohort according to the PRISM and Cancer Therapeutics Response Portal (CTRP) databases were identified (Figures S7A and S7B). We then discovered unique four PRISM-derived drugs (Triptolide, YM-155, Maytansinol, and Exatecan) and four CTRP-derived drugs (BRD9876, docetaxel, VX-680, and BRD-K30748066) by comparative analysis (logFC >0.2, $p < 0.05$) (Figures 6A and 6B). Laboratory studies reported that ribophorin II (RPN2) and budding uninhibited by BUB1 mitotic checkpoint serine/threonine kinase (BUB1) upregulation conferred the docetaxel resistance of cancer cells.[47,48] Consistent with the previous research, patients in the MPS3 subgroup had higher expression levels of the above two genes and AUC values, suggesting a lower sensitivity to docetaxel (Figure 6C).

To validate the chemotherapy sensitivity prediction ability of MPS classification, we stratified EC cell lines based on transcriptomic profiles using the pair method (Figure 6D). Metabolites differential

Figure 3. Metabolic pathway-based subtyping revealed distinct transcriptomic characteristics

(A–C) Chord diagrams displaying enriched metabolic pathways with significantly changed metabolic genes in each MPS cluster: (A) MPS1 cluster, (B) MPS2 cluster, and (C) MPS3 cluster. (D) GSEA plots of differentially changed hallmark oncogenic pathways of MPS1 and MPS3 clusters. (E) Comparison of EMT scores of each MPS cluster. ns, no significance. (F) Boxplots of comparison of EMT-related genes, *SOX9*, *TWIST1*, *FOXF1*, *ZEB1*, *ZEB2*, and *GATA6*. (G) Heatmap displaying the correlation between enrichment scores of metabolic pathways and hallmark oncogenic pathways. *$p < 0.05$; **$p < 0.01$; ***$p < 0.001$; ****$p < 0.0001$.

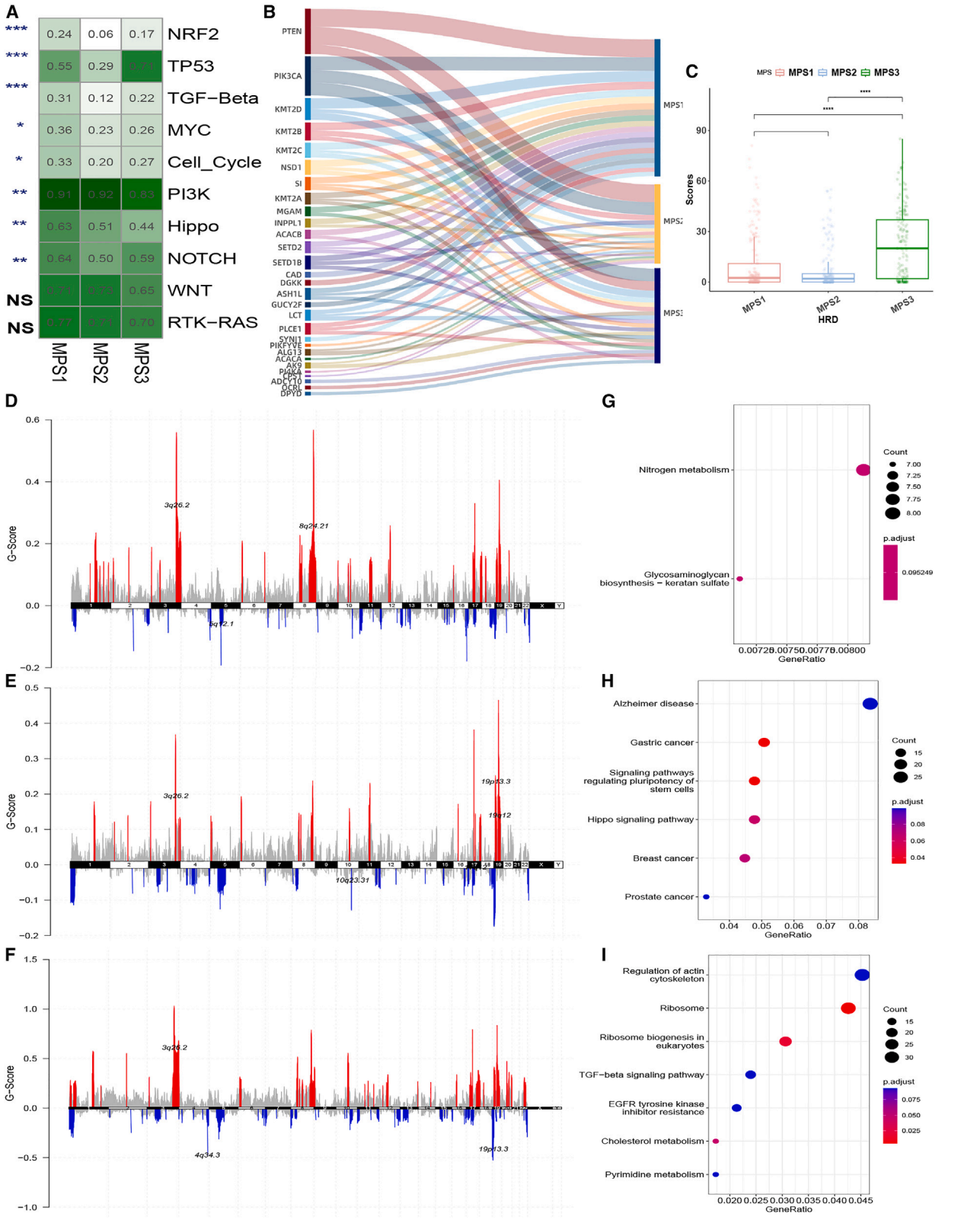

(legend on next page)

analysis revealed higher glutathione reduced, cytidine monophosphate, and triacylglycerol levels, and lower ornithine, anserine, and 3-methyl adipic acid in cell MPS3 (Figure 6E). KEGG enrichment analysis underscored the consistent enriched metabolic pathways within the cell MPS1 cluster compared with the MPS3 subgroup in the TCGA cohort, encompassing most pathways such as fructose and mannose metabolism, pyrimidine metabolism, and vitamin B_6 metabolism, thereby confirming the robustness of MPS classification in EC cell lines (Figures S7C and S7D). Next, as anticipated, the EC cell MPS3 subgroup exhibited greater aggressiveness than the MPS1 subgroup, marked by the upregulation of EMT and hedgehog pathways (Figure 6F). Furthermore, we found similar responses to MPS-unique agents between two cell MPS subgroups based on the PRISM (Figure 6G). This integrated approach, combining cellular transcriptomes and metabolomics, not only strengthens the reliability of metabolic pathway subtyping but also provides valuable insights into tailored therapeutic strategies for EC.

Development of metabolism-related prognosis risk model using machine learning algorithms

Subsequently, we sought to quantitatively assess the prognostic relevance of metabolic gene expression by using advanced machine learning techniques to develop a predictive model (Figure 7A). First, 392 metabolic genes were found to be significantly associated with OS by univariate Cox regression analysis ($p < 0.05$) (Table S7). LASSO-LR (least absolute shrinkage and selection operator regularized logistic regression) Cox regression identified 22 key genes when the lambda value was set as lambda. min (Figures 7B and S8A). The LASSO-LR model, incorporating these selected genes, demonstrated higher AUC values for 1–5 years and effectively discriminated patients' OS (Figures S8B and S8C). The optimal random forest model was achieved via grid search, setting ntree = 200 and nsplit = 5, resulting in error rates below 0.20 (Figures 7C and S8D). Internal 10-fold cross-validation further confirmed the accuracy of the random forest model, with mean C-index values of 0.72 in the training cohort and 0.60 in the testing cohort (Figure S8E). Second, 21 common metabolic genes from the LassLR and random forest models were put into stepwise regression analysis (Figures S8F and S8G). The metagene signatures were then constructed by considering all of the possible combinations (C [13, 1] + C [13, 2] + C [13, 3] + … + C [13, 13]) of the 13 selected genes using the multivariate Cox regression analysis and grouped into 5 clusters based on their respective AUC values (Figure 7D). The metagene signature 2.91*ornithine transcarbamylase (OTC) +13.23*glutamic-oxaloacetic transaminase 1 like 1 (GOT1L1) + 1.47*creatine kinase, mitochondrial 1B (CKMT1B) + 2.22*tyrosinase related protein 1 (TYRP1) + 2.29*alpha-1,3-mannosyl-glycoprotein 4-beta-N-acetylglucosaminyltransferase A (MGAT4A) + 5.59*N-deacetylase and N-sulfotransferase 4 (NDST4) + 1.62*membrane bound O-acyltransferase domain containing 2 (MBOAT2) + 0.35*PTEN +1.36*phospholipase A2 group IIA (PLA2G2A) + 0.42*tRNA selenocysteine 1 associated protein 1 (TRNAU1AP), was derived from the above 8,191 combinations with the highest C-index by 10-fold cross-validation (Figure 7E).

Based on median metagene scores, EC patients were then categorized into two groups (> median metagene scores, high risk; < median metagene scores, low risk). The time-dependent receiver operating characteristic (ROC) curves and KM survival curves also confirmed the prognosis predictive value of metagene scores ($p < 0.05$) (Figures 7F, 7G, S8H, and S8I). Furthermore, the pronounced disparity in risk scores among the MPS subgroups underscores the efficacy of the metagene signature in capturing intricate variations in tumor metabolism. The high-risk group had a comparatively higher proportion of the MPS subgroup, thereby emphasizing its utility as a tool for effectively stratifying EC cases (Figures 7H and 7I).

In our subsequent examination, we delved into the potential clinical implications of the metagene signature. Notably, the low-risk group demonstrated significantly elevated immune scores, estimate scores, and stromal scores, along with heightened CTLA4 and PDCD1 expression levels indicating a more favorable response to immunotherapy (Figures 8A and 8B). In the high-risk group, patients displayed heightened TIDE scores and lower response rates to immunotherapy across multiple cohorts, including TCGA and dependent GEO datasets such as GSE78220, GSE115821, and GSE168204. This consistent pattern reinforces the predictive utility of the metagene signature in assessing immunotherapy response (Figure 8C). Upon univariate Cox regression, patient age, Federation Internationale de Gynecolgie et d'Obstetrique (FIGO) stage, histological grade, histological type, R0 resection, tumor invasion, and metagene risk scores demonstrated significant associations with OS (Table S8). Subsequently, multivariate Cox regression was performed on the above significant features in EC patients. FIGO stage, R0 resection, and metagene risk scores were confirmed to be independently important variables of OS and then included to construct a prognostic nomogram model (Figures 8D and 8E). The nomogram model had not only good discrimination ability but also calibration ability in the training, testing, and total TCGA EC cohorts (Figures 8F and 8G).

DISCUSSION

Cancer cells not only possess a distinct metabolic profile compared to normal cells but also demonstrate significant metabolic diversity and plasticity. Cancer cell metabolism networks either directly or indirectly control key aspects of cell function covering tumor initiation,

Figure 4. Featured genomic alterations among MPS clusters in EC

(A) Comparison of mutation frequencies of 10 oncogenic pathways among the EC MPS subgroups in the TCGA cohort. (B) Sankey plot illustrating the mutation frequencies and interconnections of the top 10 differentially mutated metabolic genes in each cluster (compared with the other subgroups; false discovery rate < 0.05) in the TCGA cohort. (C) Comparison of HRD scores among MPS subgroups. (D–F) The chromosomal alteration profiles for EC MPS clusters in the TCGA cohort (D, MPS1 subgroup; E, MPS2 subgroup; F, MPS3 subgroup). (G–I) Dot plots displaying the KEGG analysis results focusing on genes located within the significantly amplified regions of each EC MPS subgroup (G, MPS1; H, MPS2; I, MPS3). *$p < 0.05$; **$p < 0.01$; ***$p < 0.001$; ****$p < 0.0001$.

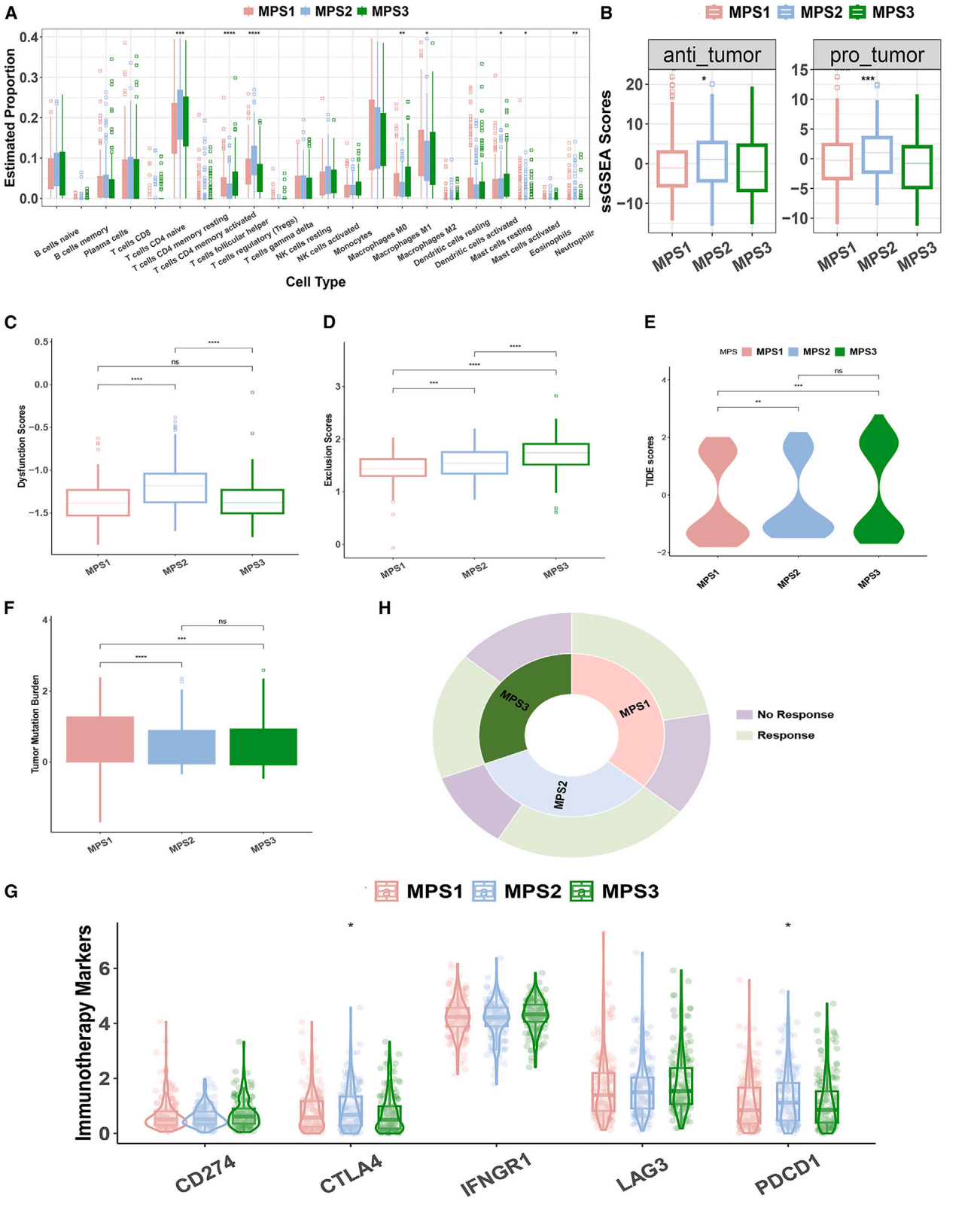

(legend on next page)

growth, and metastasis.[49] Moreover, growing evidence indicates that cancer cell metabolism has pivotal implications in the regulation of the TME immune response through the release of specific metabolites, such as lactate, prostaglandin E2, and arginine, which can influence the expression of immune molecules.[1] Understanding how cancer cells regulate their metabolic networks in heterogeneous diseases such as EC is vital for enhancing precision therapy strategies for this condition. Our research endeavors to unravel EC metabolism remodeling and heterogeneity by harnessing multi-omics and classifying ECs into three heterogeneous subtypes with distinct metabolic features, prognoses, genomic alterations, and sensitivities to various therapies (Table S9).

In alignment with prior investigations, our study illustrates that EC tissue exhibits discernible metabolic profiles compared with normal tissue at both transcriptomic and proteomic levels.[33,50] Noteworthy alterations in metabolic pathways, akin to other cancer types, encompass heightened oxidative phosphorylation, glycolysis/gluconeogenesis, and pentose and glucuronate interconversions in EC. The oxidative phosphorylation process generates ROS and drives ATP synthesis, promoting tumor initiation, proliferation, invasion, and metastasis as reported in the literature.[51–53] Cancer cells necessitate robust anabolism to synthesize essential cellular components for proliferation. In EC, this anabolic drive is evident through dysregulated biosynthetic pathways, including activated folate metabolism and diverse glycan biosynthesis. Consistent with previous studies that strengthened the significance of cytochrome P450 polymorphisms in cancer susceptibility, especially in hormone-related cancers,[54] the cytochrome P450 pathways were inactivated in EC.

Our study further corroborated the presence of metabolism heterogeneity in EC, based on a metabolism-focused transcriptional profile. EC patients in the MPS1 subgroup demonstrated a metabolism-active state supporting macromolecule synthesis, including nucleotide biosynthesis, DNA replication, and protein synthesis, under sufficient ATP and necessary substrates supply accompanied by the dysregulation of multiple metabolic pathways, such as glycolysis, one-carbon metabolism, and mitochondrial TCA cycle pathways that are known to be necessary for heme and nucleotide synthesis.[55,56] Conversely, the MPS3 subgroup showed a reduction in anabolic, energy-consuming activities, especially cell proliferation, for which EMT scores and EMT-related gene expression levels were higher, indicative of metabolism plasticity contributing to tumor metastasis. The previous literature has highlighted intrinsic metabolism reprogramming occurring in tumor cells through a slow-cycling persister state, which subsequently drives cancer progression.[57–59] Furthermore, we revealed significant disparities in drug metabolism, unsaturated fatty acid metabolism, and steroid biosynthesis pathways between the MPS2 and MPS3 subgroups, emphasizing their potential roles in determining the clinical outcomes of EC patients. Metabolomics studies also revealed that arachidonic acid, stearic acid, and linoleic acid metabolites enrolled in lipid metabolism were lowered in advanced-stage and nonendometrioid EC samples.[60–62] Building upon the insights gained from multi-omics analysis, we hypothesized that focusing on subtype-specific metabolic characteristics that significantly influence tumor behavior within the MPS subtypes may provide useful targeted therapy strategies in EC, but these need further validation in the future.

To elucidate the potential intrinsic drivers of metabolic phenotypes, we focused on germline mutations in relevant genes, including metabolic enzymes and oncogenes or tumor suppressors, as well as genomic region variations. Notably, the MPS1 subgroup exhibited higher mutation frequencies in members of the PI3K, Hippo, NRF2, and MYC pathways. These pathways increase metabolic flux to sustain proliferation through either direct regulation of nutrient transporters and metabolic enzymes or the control of transcription factors that regulate the expression of key components of metabolic pathways.[15,63,64] NRF2, a key regulator of the cellular antioxidant response, controls the expression of genes that counteract oxidative and electrophilic stresses to maintain redox homeostasis.[65,66] Moreover, we observed significant mutations in enzymes of the lysine degradation pathway, such as KMT2D/C/A and NSD1, within the MPS1 cluster. Indeed, KMT2D, a histone methyltransferase modulating chromatin structure by promoting H3K4 methylation, was frequently mutated, the loss of which induces epigenomic and metabolic reprogramming to rewire molecular pathways in multiple types of cancer.[40,67–70] In addition, the MPS3 subgroup displayed a high frequency of mutations in the TP53 pathway and had relatively heightened copy-number alterations burden and chromosomal instability. Cancer cells with homologous recombination deficiency (HRD) are particularly responsive to PARP inhibitor therapy, leveraging the vulnerability in alternative DNA repair pathways. Identifying HRD biomarkers helps pinpoint patients who can benefit from targeted PARP inhibition.[71] This study positions MPS1 as a hotspot for targeted interventions, leveraging its distinct genomic profile, while also shedding light on potential treatment avenues for the MPS3 subgroup based on chromosomal instability patterns.

Metabolism pathway-based classification also has important implications in clinical translation. First, with immune checkpoint therapy showing varying response rates, the pursuit of precision therapy becomes crucial for maximizing clinical benefits.[29,30,72] Under the circumstances, numerous studies have searched for prediction markers

Figure 5. Distinct immune microenvironment and heterogeneous responses to immunotherapy among MPSs

(A) Comparison of infiltration levels of 22 immune cells estimated by CIBERSORT analysis among the 3 MPS subgroups in the TCGA cohort. (B) The boxplot comparing the total enrichment scores of immune cells exerting antitumor (left) and protumor (right) among the 3 MPS subgroups in the TCGA cohort. (C–E) Assessment of dysfunction scores (C), exclusion scores (D), and TIDE scores (E) among the 3 MPS clusters in the TCGA cohort. (F) Boxplot displaying the total TMB among the 3 MPS subgroups in the TCGA cohort. (G) Analysis of the expression level of CD274, CTLA4, IFNGR1, LAG3, and PDCD1 in the 3 MPS subgroups of the TCGA cohort. (H) The sunburst chart displays the predictive response rate among MPS clusters in the TCGA cohort. *$p < 0.05$; **$p < 0.01$; ***$p < 0.001$; ****$p < 0.0001$.

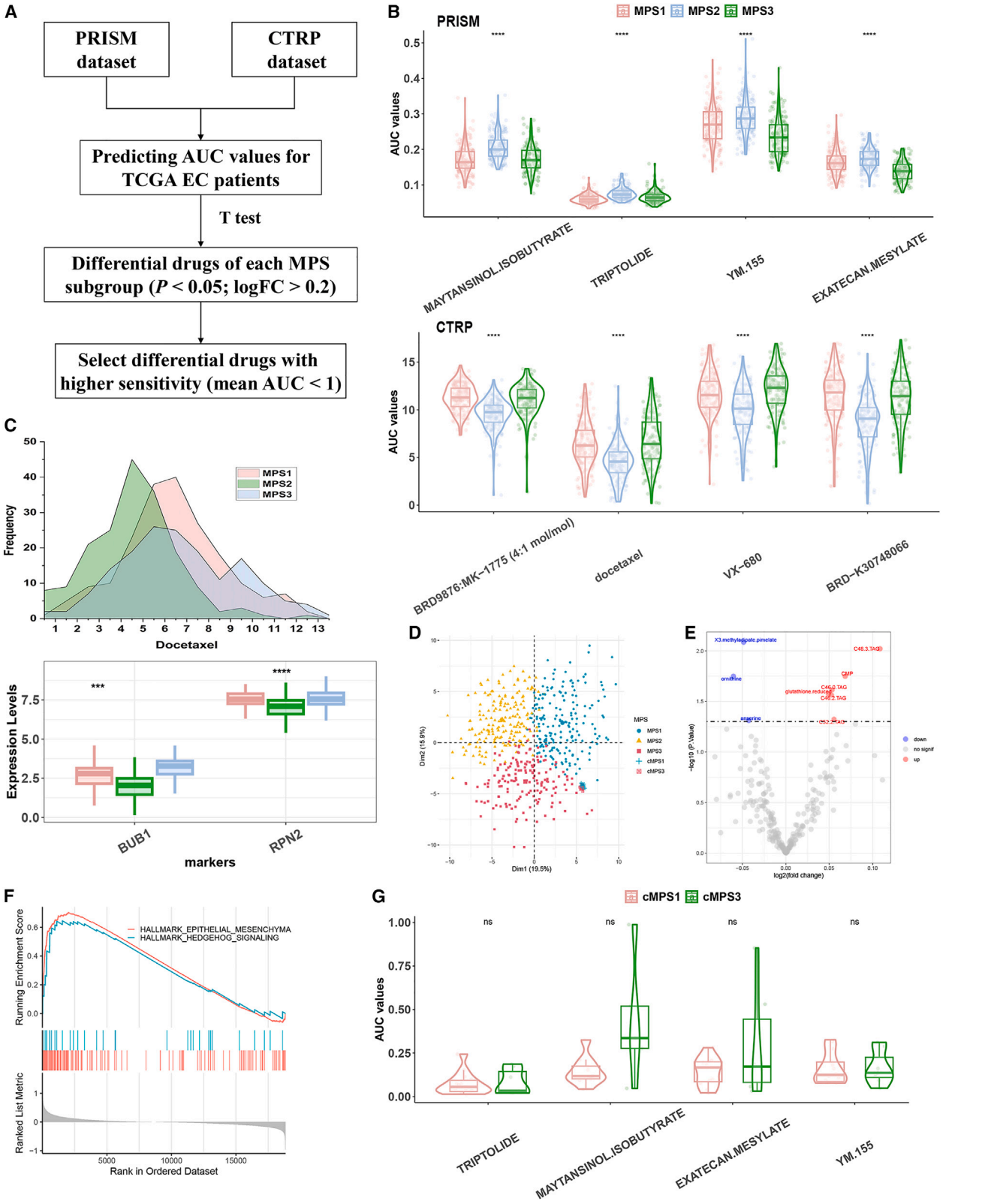

(legend on next page)

for immunotherapy response from the perspective of immune cells, molecules, and tumor mutation[73–77] More and more evidence has pointed out that tumor metabolism reprogramming has wider implications in the regulation of antitumor immune response influencing immune cell differentiation and function.[1,78,79] In our study, the MPS2 subgroup had abundant infiltration of immune cells with antitumor function and higher expression of immune molecules, whereas immune dysregulation within the TME prevented the immune cells from exerting their full effects in this subgroup. However, the MPS1 subgroup, despite having a higher TMB, showed poor immune cell infiltration, leading to a limited response to immunotherapy. Second, we demonstrated unique chemotherapeutic drug sensitivity profiles among the different MPS clusters, revealing potential therapeutic strategies tailored to tumor metabolism for treating EC patients. Intriguingly, the predicted drugs according to the CTRP database reveal rapid cell-cycle arrest in tumor cancer cells and showed higher sensitivity in the MPS1 and MPS3 clusters with lower AUC values. Furthermore, four specific drugs, exatecan mesylate, sepantronium bromide, maytansinol, and triptolide, showed promising curative effects in more aggressive EC. The exploration and analysis of high-throughput omics data under the framework of MPS subtyping not only paves the way for discovering novel drugs but also holds the promise of advancing precision clinical treatments. However, the full realization and validation of its clinical applicability require further investigation and confirmation.

The growing integration of machine learning in various healthcare domains, along with the abundance of well-characterized cancer datasets, has expedited the exploration of the potential of machine learning in deciphering the intricate biology of cancer.[80] The application of LASSO and random forest algorithms ensured the selection of important features, and stepwise regression was used to analyze the intersected variables. This process led to the identification of the optimal prognostic model for our study. The prognostic model we developed not only demonstrated robust predictive significance for patient outcomes but also facilitated the establishment of risk stratification. Furthermore, across multiple immunotherapy cohorts, our model exhibited distinct differences in immunotherapy response rates and chemotherapy outcomes, underscoring its potential clinical utility and relevance in precision medicine for cancer patients.

This study has certain limitations. First, our molecular subtyping based on metabolic pathways relied on transcriptomic data, and although we conducted external validation using other datasets and metabolomic and proteinomics data, intracohort dual validation at both transcriptomic and metabolomic levels was lacking. Second, although our metabolic subtyping showed promise in guiding clinical treatment, further rigorous clinical evaluation is needed to establish its robustness and clinical applicability. Third, although bioinformatics analysis provided insights into the associations between metabolic reprogramming and cancer genomics alterations, further mechanistic investigations are required to elucidate the precise underlying molecular mechanisms. Addressing these limitations will be crucial for advancing our understanding and application of tumor metabolism in precision medicine for EC.

MATERIALS AND METHODS

Study cohorts

Our study used multi-omics data from cohorts of EC patients extracted from the TCGA, GEO, and CPTAC datasets. Genomic (537 patients with CNV data, and 530 patients with whole-exome sequencing data), transcriptional (549 tumors and 35 normal adjacent samples), and clinical data for the TCGA cohort were downloaded from the University of California, Santa Cruz (UCSC) Xena website (https://xena.ucsc.edu/) and TCGA website (https://portal.gdc.cancer.gov/). We acquired GSE17025 (91 cancer samples and 12 samples of atrophic endometrium from postmenopausal women), GSE106191 (64 carcinoma samples and 33 hyperplasia samples), GSE29436 (4 nonprogressive EC samples and 4 progressive EC samples), GSE78220 (28 melanoma patients receiving anti-PD-1 therapy), GSE115821 (37 metastatic melanoma patients receiving immune checkpoint blockade therapy), and GSE168204 (27 melanoma patients receiving anti-PD-1 therapy) cohorts from the GEO website (https://www.ncbi.nlm.nih.gov/geo/) (Table S1). The EC proteome and corresponding clinical data were sourced from the CPTAC uterus cancer database, which includes 31 normal and 104 tumor samples (https://pdc.cancer.gov/pdc/browse).

Human EC cell lines

Transcriptomics and metabolomics data for EC cell lines were acquired from the Cancer Cell Line Encyclopedia (CCLE) website (https://sites.broadinstitute.org/ccle).[81–83] Drug sensitivity data were accessed from the CTRP2 (https://portals.broadinstitute.org/ctrp/, 481 compounds X 860 CCLs)[84–86] and the PRISM Repurposing dataset (19Q4, https://depmap.org/portal/prism/, 1448 compounds X 482 CCLs).

Data preprocessing and normalization

The fragments per kilobase of transcript per million fragments mapped data of RNA sequencing (RNA-seq) were log2 transformed and

Figure 6. Metabolism pathway-based subtyping reflects unique chemotherapy sensitivity and metabolic profiles at the cellular level

(A) Schematic outlining the strategy to develop MPS unique therapeutic agents with higher drug sensitivity in the TCGA cohort. (B) Comparison of AUC values for differentially sensitive drugs ($p < 0.05$, logFC >0.2) among each MPS subgroup based on the PRISM (upper) and CTRP (lower) database in the TCGA cohort. (C) Comparison of estimated docetaxel AUC values and its predictive gene marker expression level (BUB1 and RPN2) of each MPS in the TCGA cohort. (D) PCA plot displaying the metabolism-based subgroups of TCGA tumor samples and CCLE cell lines based on the enrichment scores of 84 metabolic pathways. (E) Volcano plot showing the differential metabolites among MPS clusters in the CCLE EC cohort ($p < 0.05$, absolute logFC >0.05). (F) GSEA plot displaying the activated hallmark pathways in the EC cell MPS3 subgroup. (G) Comparison of AUC values for differentially sensitive drugs ($p < 0.05$, logFC >0.2) among each cell line MPS subgroup based on the PRISM database in the CCLE EC. *$p < 0.05$; **$p < 0.01$; ***$p < 0.001$; ****$p < 0.0001$.

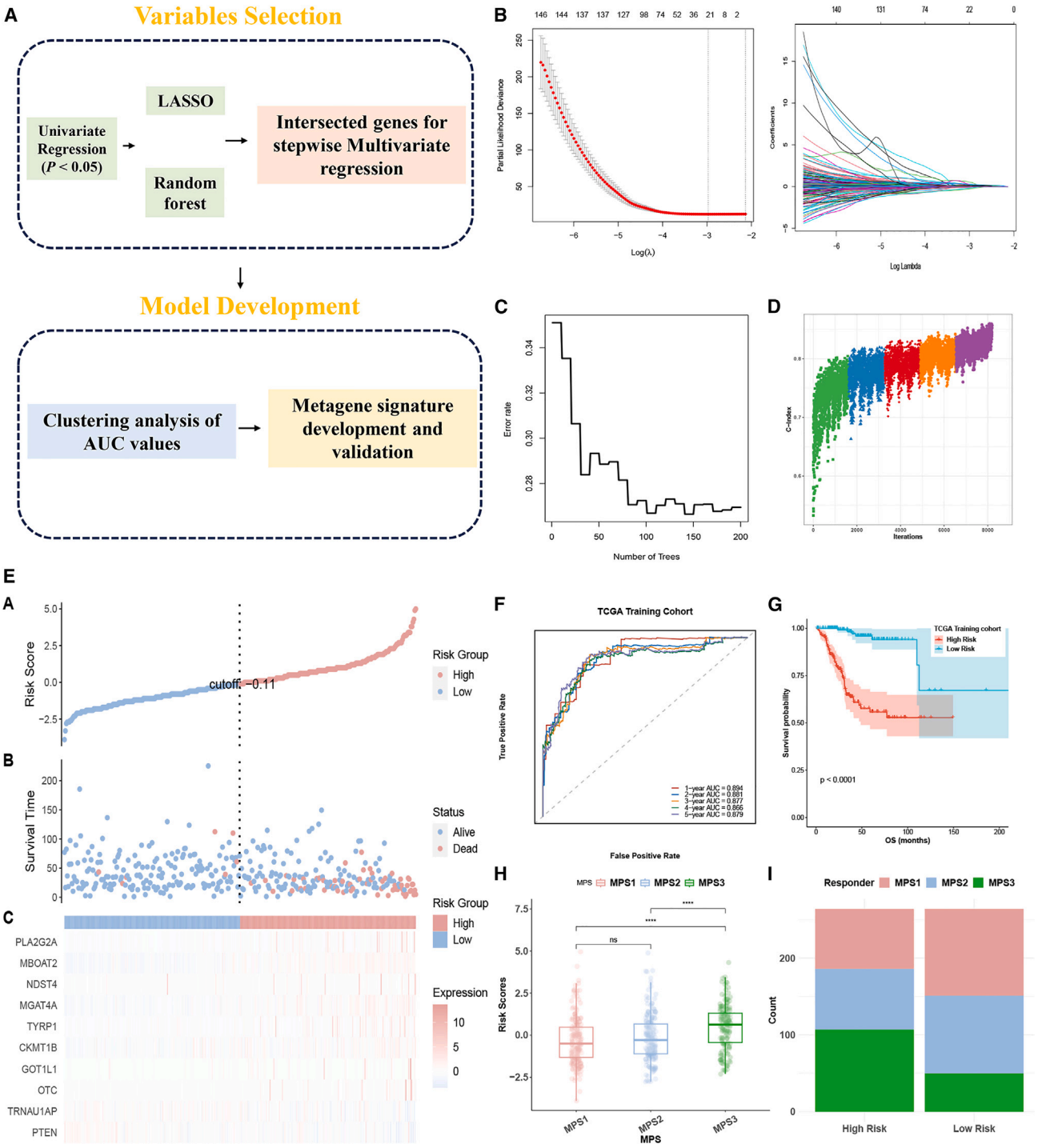

Figure 7. Development of metabolism-related prognosis risk model using machine learning algorithms

(A) The overall flowchart of metagene prognostic signature development. (B) The process of LASSO-LR model variables selection and development. (C) The plot illustrates the tuning process of the number of trees in the random forest model, with the x axis representing the number of trees and the y axis showing the corresponding error rate. (D) The mean C-index of the multivariate Cox regression model was evaluated across all of the possible combinations of the intersected genes. (E) The risk plots are composed of risk scores (A),

(legend continued on next page)

then normalized via the R package caret. For CTPAC proteomics data, the relative protein abundances were log2 transformed and zero centered for each gene to obtain final, relative abundance values. Data from the CCLE database were already preprocessed according to standard pipelines[87,88] and then scaled using the R scale method.

Calculation of metabolic and hallmark oncogenic pathways enrichment scores

Metabolic pathways were downloaded from the KEGG database (https://www.genome.jp/kegg/), including 84 metabolic pathways composed of 1,714 unique genes (Table S2). These pathways were clustered into 10 categories according to KEGG classifications. The hallmark oncogenic gene sets were downloaded from the GSEA MSigDB website (http://www.gsea-msigdb.org/gsea). We performed GSVA to calculate enrichment scores of the above pathways using the transcriptomic data of each EC sample.

PCA

We applied PCA on the TCGA EC metabolism pathway-related gene expression data and used the fviz_pca_ind function from the R package factoextra to visualize the distinct clustering patterns concerning clinical phenotypes.

GSEA

Differential gene analyses were conducted using either the R Deseq2 or limma package to produce ranked gene lists for both the TCGA and GEO datasets. Subsequently, GSEA was performed on DEGs by the R clusterProfiler package based on 84 metabolism-related and hallmark oncogenic gene sets.

Metabolic pathway-based clustering subgroups of EC

We scaled the metabolism pathway enrichment scores of each sample before clustering. The consensus ClusterPlus function was used for determining MPS clustering number and class membership by stability evidence (R ConsensusClusterPlus package, k-means clustering, pItem = 0.8, pFeature = 1). In this study, we also performed NbClust testing (Euclidean distance, k-means, from 2 to 15 clusters) to confirm the best number of clusters based on EC metabolism-pathway enrichment scores by varying all of the combinations of the number of clusters by the R NbClust package.

Clinical characteristics analysis among MPS clusters

The FIGO stage, histological type, histological grade, four TCGA molecular subgroups,[24] and patient age were compared among MPS clusters. KM survival plots were generated to assess the differences in OS and DFS among different MPS clusters using the R packages survival and survminer. In addition, univariate and multivariate Cox proportional hazard regression analyses were conducted to validate the prognostic value of MPS subgroups.

EMT scores calculation

The gene signatures for the EMT were obtained from Mak et al.,[89] which included 25 epithelial marker genes and 52 mesenchymal marker genes. The EMT score for each sample was calculated as described using the formula $\sum_i^N \frac{M_i}{N} - \sum_i^n \frac{E_i}{n}$, where M and E represent the expression of mesenchymal and epithelial genes, respectively, and N and n are the total numbers of mesenchymal and epithelial genes, respectively.

Comparison of gene mutation frequencies among subgroups

The top 10 genes with the highest mutation frequency were identified in different MPS clusters by the R maftools package. For each cluster, the fraction of samples with at least one alteration in 10 canonical oncogenic pathways cell cycle, Hippo, Myc, Notch, Nrf2, PI3K/Akt, RTK-RAS, TGF-β signaling, p53, and β-catenin/Wnt was compared.[38] We also performed pairwise and groupwise Fisher exact tests to find differentially enriched metabolic genes for every MPS subgroup.

Identification of genomic alterations and potential functions of MPS clusters

The TCGA CNV data were annotated according to the hg38 genome and analyzed by the online GISTIC2 module on the Genepattern website (https://cloud.genepattern.org/) to detect regions with amplification or deletion. Genes with q values <0.25 were annotated as amplified (G scores >0) or deleted (G scores <0) and subjected to functional annotation by KEGG pathway analysis using the R clusterProfiler package. HRD scores, calculated by the sum of the loss of heterozygosity score, allelic imbalance extending to the telomere score, and large-scale state transition score, were compared among MPS subgroups.[90]

Tumor immune microenvironment infiltration analysis

To investigate tumor immune cell infiltration, we used the R CIBERSORT analysis among different MPS clusters.[91] Specifically, we focused on four aggregated immune cell types: total lymphocytes, total dendritic cells (sum of activated and resting dendritic cell percentages), total macrophages (sum of M0, M1, and M2 macrophages), and total mast cells (sum of activated and resting mast cell percentages). Moreover, we calculated the M1 to M2 ratio as the ratio between the M1 macrophage percentage and the M2 macrophage percentage.

We also used ssGSEA algorithms to calculate 28 immune cell enrichment scores and summed scores of antitumor immune cells (the

survival status (B), and gene expression level (C) of metagene signature. (F) Time-dependent ROC curves of the metagene signature for predicting OS in the TCGA training cohort. (G) KM curves distinguished OS well between the high-risk group and the low-risk group based on the metagene signature in the TCGA training cohort. (H) Comparison of metagene risk scores among 3 MPS subgroups in the TCGA cohort. (I) The stacked bar plot displays the composition of MPS subgroups in the metagene high-risk and low-risk groups in the TCGA cohort.

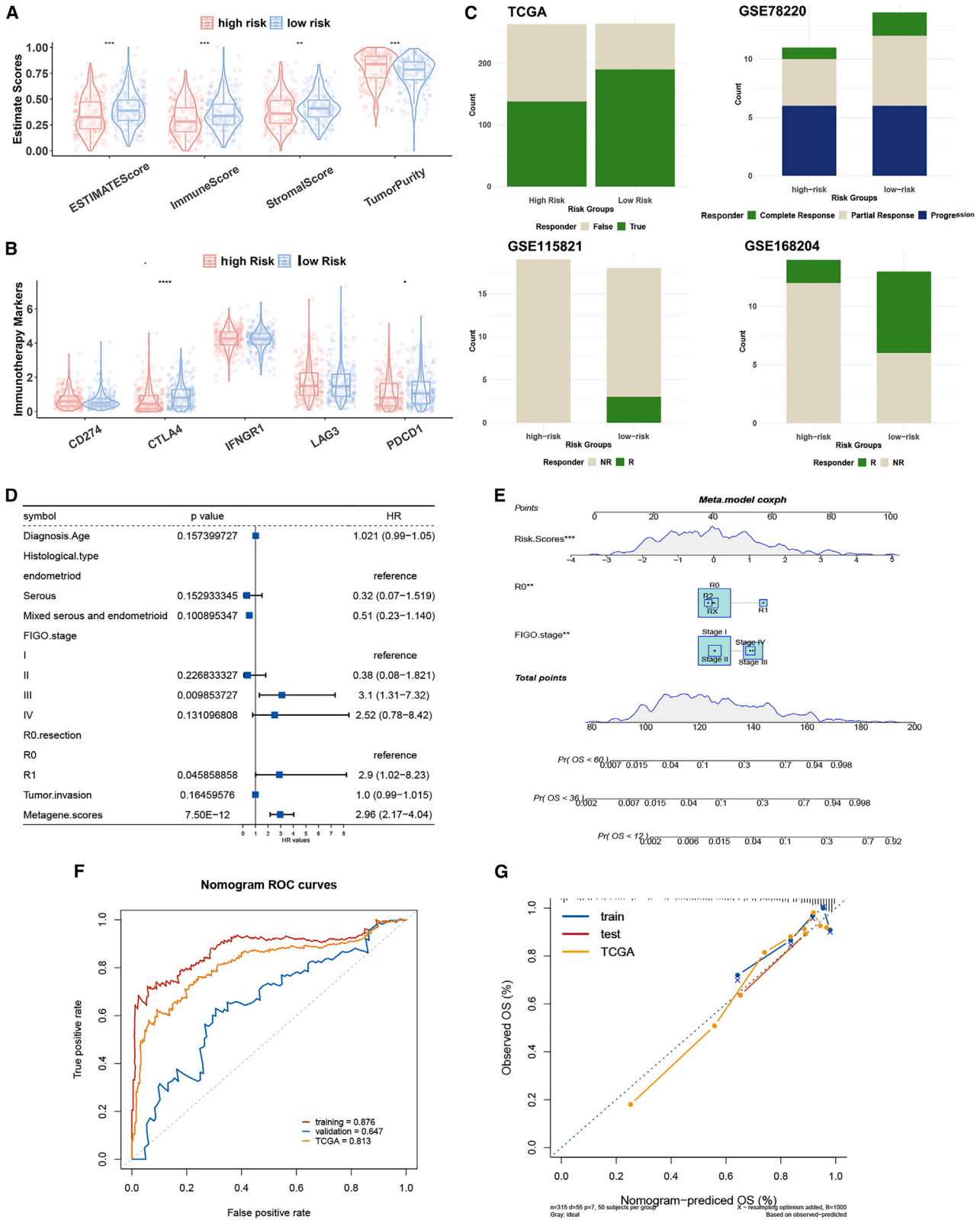

(legend on next page)

aggregation of activated CD4 T cell, activated CD8 T cell, central memory CD4 T cell, central memory CD8 T cell, effector memory CD4 T cell, effector memory CD8 T cell, type 1 T helper cell, type 17 T helper cell, activated dendritic cell, CD56bright natural killer cell, natural killer cell, and natural killer T cell) and protumor immune cells (regulatory T cell, type 2 T helper cell, CD56dim natural killer cell, immature dendritic cell, macrophage, myeloid-derived suppressor cell, neutrophil, and plasmacytoid dendritic cell).[92]

Immunotherapy response prediction

TIDE is an algorithm based on the expression pattern of multiple immune-related genes, including T cell immunity, B cell immunity, antigen processing, and presentation pathways.[93] We uploaded EC RNA-seq data to the TIDE website to compare the TIDE scores among different clusters. In addition, we compared the gene expression levels of immune checkpoint molecules, TMB levels, and immune cell levels among MPS clusters to predict immunotherapy response.

Drug sensitivity prediction based on RNAseq data

The CTRP and PRISM datasets use the area under the dose-response curve values as a measure of drug sensitivity, in which lower AUC values indicated increased sensitivity to treatment.[86] The R package oncoPredict was used to predict the drug sensitivity of each patient in TCGA cohort based on the above datasets. We used the Student's t test to identify drugs with significant differences in efficacy across different MPS subgroups. Drugs exhibiting a $p < 0.05$ and $log2FC > 0.2$ were selected as potential drugs for further analysis.

EC cell lines classification

The enrichment scores of the metabolic pathways using the GSVA method as above described were initially calculated based on the CCLE EC transcriptomic profiles. Then, we extrapolated metabolism-based classification to EC cell lines by the pamr.train and pamr. predict functions of the R pamr package using the nearest shrunken centroid classifier.

Pathway enrichment analysis of EC cell lines metabolomics data

MetaboAnalyst (https://www.metaboanalyst.ca/) provides a user-friendly web interface that allows us to upload metabolomics data and perform pathway enrichment analysis using various databases based on compound concentration values.[94]

Machine learning algorithms for metabolic prognostic model construction

The TCGA EC cohort was randomly divided into training and testing cohorts in a 7:3 ratio. The predictive model was constructed as follows: (1) univariate Cox regression analysis was performed on 1,714 metabolic genes to identify prognosis-significant genes in the training cohort ($p < 0.05$). (2) LASSO-LR and random forest were separately used to select features for model development. Each algorithm was tried with different parameter combinations. (3) The common genes identified by the above two methods were subjected to multivariate Cox regression analysis, followed by a backward stepwise variable selection process. (4) Metagene signatures were constructed by considering all of the possible combinations of the selected genes, weighted by their estimated regression coefficients in the multivariate Cox regression analysis.

Statistical analysis

The statistical analysis was completed using the R version (4.2.1). For binary categorical variables, the Wilcoxon rank-sum test was used to compare groups, and the Kruskal-Wallis test was used for multiclass comparisons. KM survival analysis was used for survival assessments. Univariate Cox regression analysis was used to identify prognosis-significant variables, whereas a multivariate Cox regression model was constructed to develop the predictive model. Variables with a $p < 0.05$ were deemed statistically significant.

DATA AND CODE AVAILABILITY

The TCGA cohorts were downloaded from the UCSC Xena website and the TCGA website. The GSE17025, GSE106191, GSE29436, GSE78220, GSE115821, and GSE168204 cohorts were available from the GEO website. The EC proteome and corresponding clinical data were sourced from the CPTAC uterus cancer database. The EC cell lines transcriptomics and metabolomics data were downloaded from the CCLE website.

SUPPLEMENTAL INFORMATION

Supplemental information can be found online at https://doi.org/10.1016/j.omtn.2024.102155.

ACKNOWLEDGMENTS

The study was funded by the National Natural Science Foundation of China (82273052), National High-Level Hospital Clinical Research Funding (2022-NHLHCRF-PY-13), and the Capital's Funds for Health Improvement and Research (2022-2-4063).

AUTHOR CONTRIBUTIONS

All of the authors contributed to the original ideas and writing of this paper. X.L. contributed to data collection, statistical analysis, and paper writing. X.L., X.Z., and D.F. wrote the paper. W.W., Y.L., and M.X.

Figure 8. Validation of the clinical utility of metabolism-based prognostic signature

(A and B) Comparison of estimated immune scores (A) and immunotherapy marker expression levels (B) in 2 groups divided by the metagene risk scores. (C) The stacked bar plots illustrate the immunotherapy response rates across the TCGA, GSE78220, GSE115821, and GSE168204 cohorts. (D) The forest plot displays the multivariate Cox regression analysis on OS significant variables, including patient age, histological type, FIGO stage, R0 resection status, tumor invasion percentage, and metagene scores. (E) Nomogram plot of the multivariate Cox regression model for predicting EC OS. (F) The 5-year ROC curves of the nomogram predictive model in the training, testing, and TCGA EC cohorts. (G) The 5-year calibration curves of the nomogram predictive model in the training, testing, and TCGA EC cohorts demonstrated higher consistency with the observed outcome. *$p < 0.05$; **$p < 0.01$; ***$p < 0.001$; ****$p < 0.0001$.

drew the figures. B.L., J.L., and D.F. made critical revisions to this paper. All of the authors read and approved the final manuscript.

DECLARATION OF INTERESTS

The authors declare no competing interests.

REFERENCES

1. Xia, L., Oyang, L., Lin, J., Tan, S., Han, Y., Wu, N., Yi, P., Tang, L., Pan, Q., Rao, S., et al. (2021). The cancer metabolic reprogramming and immune response. Mol. Cancer *20*, 28.
2. Warburg, O. (1956). On the origin of cancer cells. Science (New York, N.Y.) *123*, 309–314.
3. Vander Heiden, M.G., Cantley, L.C., and Thompson, C.B. (2009). Understanding the Warburg effect: the metabolic requirements of cell proliferation. Science (New York, N.Y.) *324*, 1029–1033.
4. Vander Heiden, M.G., and DeBerardinis, R.J. (2017). Understanding the Intersections between Metabolism and Cancer Biology. Cell *168*, 657–669.
5. Ghergurovich, J.M., Lang, J.D., Levin, M.K., Briones, N., Facista, S.J., Mueller, C., Cowan, A.J., McBride, M.J., Rodriguez, E.S.R., Killian, A., et al. (2021). Local production of lactate, ribose phosphate, and amino acids within human triple-negative breast cancer. Méd. *2*, 736–754.
6. Knott, S.R.V., Wagenblast, E., Khan, S., Kim, S.Y., Soto, M., Wagner, M., Turgeon, M.O., Fish, L., Erard, N., Gable, A.L., et al. (2018). Asparagine bioavailability governs metastasis in a model of breast cancer. Nature *554*, 378–381.
7. Eniafe, J., and Jiang, S. (2021). The functional roles of TCA cycle metabolites in cancer. Oncogene *40*, 3351–3363.
8. Sellers, K., Fox, M.P., Bousamra, M., 2nd, Slone, S.P., Higashi, R.M., Miller, D.M., Wang, Y., Yan, J., Yuneva, M.O., Deshpande, R., et al. (2015). Pyruvate carboxylase is critical for non-small-cell lung cancer proliferation. J. Clin. Invest. *125*, 687–698.
9. Christen, S., Lorendeau, D., Schmieder, R., Broekaert, D., Metzger, K., Veys, K., Elia, I., Buescher, J.M., Orth, M.F., Davidson, S.M., et al. (2016). Breast Cancer-Derived Lung Metastases Show Increased Pyruvate Carboxylase-Dependent Anaplerosis. Cell Rep. *17*, 837–848.
10. Faubert, B., Solmonson, A., and DeBerardinis, R.J. (2020). Metabolic reprogramming and cancer progression. Science *368*, eaaw5473.
11. Losman, J.A., Looper, R.E., Koivunen, P., Lee, S., Schneider, R.K., McMahon, C., Cowley, G.S., Root, D.E., Ebert, B.L., and Kaelin, W.G., Jr. (2013). (R)-2-hydroxyglutarate is sufficient to promote leukemogenesis and its effects are reversible. Science (New York, N.Y.) *339*, 1621–1625.
12. Martínez-Reyes, I., and Chandel, N.S. (2020). Mitochondrial TCA cycle metabolites control physiology and disease. Nat. Commun. *11*, 102.
13. Zhang, D., Tang, Z., Huang, H., Zhou, G., Cui, C., Weng, Y., Liu, W., Kim, S., Lee, S., Perez-Neut, M., et al. (2019). Metabolic regulation of gene expression by histone lactylation. Nature *574*, 575–580.
14. Lacroix, M., Riscal, R., Arena, G., Linares, L.K., and Le Cam, L. (2020). Metabolic functions of the tumor suppressor p53: Implications in normal physiology, metabolic disorders, and cancer. Mol. Metabol. *33*, 2–22.
15. Carroll, P.A., Freie, B.W., Mathsyaraja, H., and Eisenman, R.N. (2018). The MYC transcription factor network: balancing metabolism, proliferation and oncogenesis. Front. Med. *12*, 412–425.
16. Liu, G.Y., and Sabatini, D.M. (2020). mTOR at the nexus of nutrition, growth, ageing and disease. Nat. Rev. Mol. Cell Biol. *21*, 183–203.
17. Ali, E.S., Sahu, U., Villa, E., O'Hara, B.P., Gao, P., Beaudet, C., Wood, A.W., Asara, J.M., and Ben-Sahra, I. (2020). ERK2 Phosphorylates PFAS to Mediate Posttranslational Control of De Novo Purine Synthesis. Mol. Cell *78*, 1178–1191.e6.
18. Gong, Y., Ji, P., Yang, Y.S., Xie, S., Yu, T.J., Xiao, Y., Jin, M.L., Ma, D., Guo, L.W., Pei, Y.C., et al. (2021). Metabolic-Pathway-Based Subtyping of Triple-Negative Breast Cancer Reveals Potential Therapeutic Targets. Cell Metabol. *33*, 51–64.e9.
19. Yu, T.J., Ma, D., Liu, Y.Y., Xiao, Y., Gong, Y., Jiang, Y.Z., Shao, Z.M., Hu, X., and Di, G.H. (2021). Bulk and single-cell transcriptome profiling reveal the metabolic heterogeneity in human breast cancers. Mol. Ther. *29*, 2350–2365.
20. Chen, D., Zhang, Y., Wang, W., Chen, H., Ling, T., Yang, R., Wang, Y., Duan, C., Liu, Y., Guo, X., et al. (2021). Identification and Characterization of Robust Hepatocellular Carcinoma Prognostic Subtypes Based on an Integrative Metabolite-Protein Interaction Network. Adv. Sci. *8*, e2100311.
21. McBrayer, S.K., Mayers, J.R., DiNatale, G.J., Shi, D.D., Khanal, J., Chakraborty, A.A., Sarosiek, K.A., Briggs, K.J., Robbins, A.K., Sewastianik, T., et al. (2018). Transaminase Inhibition by 2-Hydroxyglutarate Impairs Glutamate Biosynthesis and Redox Homeostasis in Glioma. Cell *175*, 101–116.e25.
22. Daneshmandi, S., Wegiel, B., and Seth, P. (2019). Blockade of Lactate Dehydrogenase-A (LDH-A) Improves Efficacy of Anti-Programmed Cell Death-1 (PD-1) Therapy in Melanoma. Cancers *11*, 450.
23. Hangauer, M.J., Viswanathan, V.S., Ryan, M.J., Bole, D., Eaton, J.K., Matov, A., Galeas, J., Dhruv, H.D., Berens, M.E., Schreiber, S.L., et al. (2017). Drug-tolerant persister cancer cells are vulnerable to GPX4 inhibition. Nature *551*, 247–250.
24. Cancer Genome Atlas Research Network, Kandoth, C., Schultz, N., Cherniack, A.D., Akbani, R., Liu, Y., Shen, H., Robertson, A.G., Pashtan, I., Shen, R., et al. (2013). Integrated genomic characterization of endometrial carcinoma. Nature *497*, 67–73.
25. Sung, H., Ferlay, J., Siegel, R.L., Laversanne, M., Soerjomataram, I., Jemal, A., and Bray, F. (2021). Global Cancer Statistics 2020: GLOBOCAN Estimates of Incidence and Mortality Worldwide for 36 Cancers in 185 Countries. CA A Cancer J. Clin. *71*, 209–249.
26. Gu, B., Shang, X., Yan, M., Li, X., Wang, W., Wang, Q., and Zhang, C. (2021). Variations in incidence and mortality rates of endometrial cancer at the global, regional, and national levels, 1990-2019. Gynecol. Oncol. *161*, 573–580.
27. Britton, H., Huang, L., Lum, A., Leung, S., Shum, K., Kale, M., Burleigh, A., Senz, J., Yang, W., McConechy, M., et al. (2019). Molecular classification defines outcomes and opportunities in young women with endometrial carcinoma. Gynecol. Oncol. *153*, 487–495.
28. Soliman, P.T., Westin, S.N., Iglesias, D.A., Fellman, B.M., Yuan, Y., Zhang, Q., Yates, M.S., Broaddus, R.R., Slomovitz, B.M., Lu, K.H., and Coleman, R.L. (2020). Everolimus, Letrozole, and Metformin in Women with Advanced or Recurrent Endometrioid Endometrial Cancer: A Multi-Center, Single Arm, Phase II Study. Clin. Cancer Res. *26*, 581–587.
29. Ott, P.A., Bang, Y.J., Berton-Rigaud, D., Elez, E., Pishvaian, M.J., Rugo, H.S., Puzanov, I., Mehnert, J.M., Aung, K.L., Lopez, J., et al. (2017). Safety and Antitumor Activity of Pembrolizumab in Advanced Programmed Death Ligand 1-Positive Endometrial Cancer: Results From the KEYNOTE-028 Study. J. Clin. Oncol. *35*, 2535–2541.
30. Oaknin, A., Tinker, A.V., Gilbert, L., Samouëlian, V., Mathews, C., Brown, J., Barretina-Ginesta, M.P., Moreno, V., Gravina, A., Abdeddaim, C., et al. (2020). Clinical Activity and Safety of the Anti-Programmed Death 1 Monoclonal Antibody Dostarlimab for Patients With Recurrent or Advanced Mismatch Repair-Deficient Endometrial Cancer: A Nonrandomized Phase 1 Clinical Trial. JAMA Oncol. *6*, 1766–1772.
31. Raglan, O., Kalliala, I., Markozannes, G., Cividini, S., Gunter, M.J., Nautiyal, J., Gabra, H., Paraskevaidis, E., Martin-Hirsch, P., Tsilidis, K.K., and Kyrgiou, M. (2019). Risk factors for endometrial cancer: An umbrella review of the literature. Int. J. Cancer *145*, 1719–1730.
32. Dossus, L., Kouloura, E., Biessy, C., Viallon, V., Siskos, A.P., Dimou, N., Rinaldi, S., Merritt, M.A., Allen, N., Fortner, R., et al. (2021). Prospective analysis of circulating metabolites and endometrial cancer risk. Gynecol. Oncol. *162*, 475–481.
33. Yang, X., Cheng, Y., Zhou, J., Zhang, L., Li, X., Wang, Z., Yin, S., Zhai, L., Huang, T., Wu, X., et al. (2022). Targeting Cancer Metabolism Plasticity with JX06 Nanoparticles via Inhibiting PDK1 Combined with Metformin for Endometrial Cancer Patients with Diabetes. Adv. Sci. *9*, e2104472.
34. Jamieson, A., and McAlpine, J.N. (2023). Molecular Profiling of Endometrial Cancer From TCGA to Clinical Practice. J. Natl. Compr. Cancer Netw. *21*, 210–216.
35. Lee, S.Y., Jeong, E.K., Ju, M.K., Jeon, H.M., Kim, M.Y., Kim, C.H., Park, H.G., Han, S.I., and Kang, H.S. (2017). Induction of metastasis, cancer stem cell phenotype, and oncogenic metabolism in cancer cells by ionizing radiation. Mol. Cancer *16*, 10.

36. Nava Lauson, C.B., Tiberti, S., Corsetto, P.A., Conte, F., Tyagi, P., Machwirth, M., Ebert, S., Loffreda, A., Scheller, L., Sheta, D., et al. (2023). Linoleic acid potentiates CD8(+) T cell metabolic fitness and antitumor immunity. Cell Metabol. *35*, 633–650.e9.

37. Stine, Z.E., Schug, Z.T., Salvino, J.M., and Dang, C.V. (2022). Targeting cancer metabolism in the era of precision oncology. Nat. Rev. Drug Discov. *21*, 141–162.

38. Sanchez-Vega, F., Mina, M., Armenia, J., Chatila, W.K., Luna, A., La, K.C., Dimitriadoy, S., Liu, D.L., Kantheti, H.S., Saghafinia, S., et al. (2018). Oncogenic Signaling Pathways in The Cancer Genome Atlas. Cell *173*, 321–337.e10.

39. Husmann, D., and Gozani, O. (2019). Histone lysine methyltransferases in biology and disease. Nat. Struct. Mol. Biol. *26*, 880–889.

40. Alam, H., Tang, M., Maitituoheti, M., Dhar, S.S., Kumar, M., Han, C.Y., Ambati, C.R., Amin, S.B., Gu, B., Chen, T.Y., et al. (2020). KMT2D Deficiency Impairs Super-Enhancers to Confer a Glycolytic Vulnerability in Lung Cancer. Cancer Cell *37*, 599–617.e7.

41. Siedel, J.H., Ring, K.L., Hu, W., Dood, R.L., Wang, Y., Baggerly, K., Darcy, K.M., Conrads, T.P., Gallagher, S., Tshiaba, P., et al. (2021). Clinical significance of homologous recombination deficiency score testing in endometrial Cancer. Gynecol. Oncol. *160*, 777–785.

42. Telli, M.L., Timms, K.M., Reid, J., Hennessy, B., Mills, G.B., Jensen, K.C., Szallasi, Z., Barry, W.T., Winer, E.P., Tung, N.M., et al. (2016). Homologous Recombination Deficiency (HRD) Score Predicts Response to Platinum-Containing Neoadjuvant Chemotherapy in Patients with Triple-Negative Breast Cancer. Clin. Cancer Res. *22*, 3764–3773.

43. Apostolova, P., and Pearce, E.L. (2022). Lactic acid and lactate: revisiting the physiological roles in the tumor microenvironment. Trends Immunol. *43*, 969–977.

44. Dyck, L., and Lynch, L. (2023). Diverse effects of obesity on antitumor immunity and immunotherapy. Trends Mol. Med. *29*, 112–123.

45. Chow, R.D., Michaels, T., Bellone, S., Hartwich, T.M.P., Bonazzoli, E., Iwasaki, A., Song, E., and Santin, A.D. (2023). Distinct Mechanisms of Mismatch-Repair Deficiency Delineate Two Modes of Response to Anti-PD-1 Immunotherapy in Endometrial Carcinoma. Cancer Discov. *13*, 312–331.

46. Shen, R., Postow, M.A., Adamow, M., Arora, A., Hannum, M., Maher, C., Wong, P., Curran, M.A., Hollmann, T.J., Jia, L., et al. (2021). LAG-3 expression on peripheral blood cells identifies patients with poorer outcomes after immune checkpoint blockade. Sci. Transl. Med. *13*, eabf5107.

47. Honma, K., Iwao-Koizumi, K., Takeshita, F., Yamamoto, Y., Yoshida, T., Nishio, K., Nagahara, S., Kato, K., and Ochiya, T. (2008). RPN2 gene confers docetaxel resistance in breast cancer. Nat. Med. *14*, 939–948.

48. Chen, L., Song, Y., Hou, T., Li, X., Cheng, L., Li, Y., and Xing, Y. (2022). Circ_0004087 interaction with SND1 promotes docetaxel resistance in prostate cancer by boosting the mitosis error correction mechanism. J. Exp. Clin. Cancer Res. *41*, 194.

49. Finley, L.W.S. (2023). What is cancer metabolism? Cell *186*, 1670–1688.

50. Huang, P., Fan, X., Yu, H., Zhang, K., Li, H., Wang, Y., and Xue, F. (2023). Glucose metabolic reprogramming and its therapeutic potential in obesity-associated endometrial cancer. J. Transl. Med. *21*, 94.

51. Cheung, E.C., DeNicola, G.M., Nixon, C., Blyth, K., Labuschagne, C.F., Tuveson, D.A., and Vousden, K.H. (2020). Dynamic ROS Control by TIGAR Regulates the Initiation and Progression of Pancreatic Cancer. Cancer Cell *37*, 168–182.e4.

52. DeNicola, G.M., Karreth, F.A., Humpton, T.J., Gopinathan, A., Wei, C., Frese, K., Mangal, D., Yu, K.H., Yeo, C.J., Calhoun, E.S., et al. (2011). Oncogene-induced Nrf2 transcription promotes ROS detoxification and tumorigenesis. Nature *475*, 106–109.

53. Woo, D.K., Green, P.D., Santos, J.H., D'Souza, A.D., Walther, Z., Martin, W.D., Christian, B.E., Chandel, N.S., and Shadel, G.S. (2012). Mitochondrial genome instability and ROS enhance intestinal tumorigenesis in APC(Min/+) mice. Am. J. Pathol. *180*, 24–31.

54. Mittal, B., Tulsyan, S., Kumar, S., Mittal, R.D., and Agarwal, G. (2015). Cytochrome P450 in Cancer Susceptibility and Treatment. Adv. Clin. Chem. *71*, 77–139.

55. Martínez-Reyes, I., Cardona, L.R., Kong, H., Vasan, K., McElroy, G.S., Werner, M., Kihshen, H., Reczek, C.R., Weinberg, S.E., Gao, P., et al. (2020). Mitochondrial ubiquinol oxidation is necessary for tumour growth. Nature *585*, 288–292.

56. Ducker, G.S., Chen, L., Morscher, R.J., Ghergurovich, J.M., Esposito, M., Teng, X., Kang, Y., and Rabinowitz, J.D. (2016). Reversal of Cytosolic One-Carbon Flux Compensates for Loss of the Mitochondrial Folate Pathway. Cell Metabol. *23*, 1140–1153.

57. Bartman, C.R., Weilandt, D.R., Shen, Y., Lee, W.D., Han, Y., TeSlaa, T., Jankowski, C.S.R., Samarah, L., Park, N.R., da Silva-Diz, V., et al. (2023). Slow TCA flux and ATP production in primary solid tumours but not metastases. Nature *614*, 349–357.

58. Ravindran Menon, D., Hammerlindl, H., Torrano, J., Schaider, H., and Fujita, M. (2020). Epigenetics and metabolism at the crossroads of stress-induced plasticity, stemness and therapeutic resistance in cancer. Theranostics *10*, 6261–6277.

59. Kiweler, N., Delbrouck, C., Pozdeev, V.I., Neises, L., Soriano-Baguet, L., Eiden, K., Xian, F., Benzarti, M., Haase, L., Koncina, E., et al. (2022). Mitochondria preserve an autarkic one-carbon cycle to confer growth-independent cancer cell migration and metastasis. Nat. Commun. *13*, 2699.

60. Gu, M., Chen, X., Sun, Y., Wang, L., Shu, H., and Qian, C. (2021). A metabolomic signature of FIGO stage I and II endometrial cancer. Neoplasma *68*, 1283–1291.

61. Audet-Delage, Y., Villeneuve, L., Grégoire, J., Plante, M., and Guillemette, C. (2018). Identification of Metabolomic Biomarkers for Endometrial Cancer and Its Recurrence after Surgery in Postmenopausal Women. Front. Endocrinol. *9*, 87.

62. Gatius, S., Jove, M., Megino-Luque, C., Albertí-Valls, M., Yeramian, A., Bonifaci, N., Piñol, M., Santacana, M., Pradas, I., Llobet-Navas, D., et al. (2022). Metabolomic Analysis Points to Bioactive Lipid Species and Acireductone Dioxygenase 1 (ADI1) as Potential Therapeutic Targets in Poor Prognosis Endometrial Cancer. Cancers *14*, 2842.

63. Hoxhaj, G., and Manning, B.D. (2020). The PI3K-AKT network at the interface of oncogenic signalling and cancer metabolism. Nat. Rev. Cancer *20*, 74–88.

64. Ji, S., Liu, Q., Zhang, S., Chen, Q., Wang, C., Zhang, W., Xiao, C., Li, Y., Nian, C., Li, J., et al. (2019). FGF15 Activates Hippo Signaling to Suppress Bile Acid Metabolism and Liver Tumorigenesis. Dev. Cell *48*, 460–474.e9.

65. Dodson, M., Castro-Portuguez, R., and Zhang, D.D. (2019). NRF2 plays a critical role in mitigating lipid peroxidation and ferroptosis. Redox Biol. *23*, 101107.

66. Lignitto, L., LeBoeuf, S.E., Homer, H., Jiang, S., Askenazi, M., Karakousi, T.R., Pass, H.I., Bhutkar, A.J., Tsirigos, A., Ueberheide, B., et al. (2019). Nrf2 Activation Promotes Lung Cancer Metastasis by Inhibiting the Degradation of Bach1. Cell *178*, 316–329.e18.

67. Rao, R.C., and Dou, Y. (2015). Hijacked in cancer: the KMT2 (MLL) family of methyltransferases. Nat. Rev. Cancer *15*, 334–346.

68. Wang, G., Chow, R.D., Zhu, L., Bai, Z., Ye, L., Zhang, F., Renauer, P.A., Dong, M.B., Dai, X., Zhang, X., et al. (2020). CRISPR-GEMM Pooled Mutagenic Screening Identifies KMT2D as a Major Modulator of Immune Checkpoint Blockade. Cancer Discov. *10*, 1912–1933.

69. Zhang, Y., Donaher, J.L., Das, S., Li, X., Reinhardt, F., Krall, J.A., Lambert, A.W., Thiru, P., Keys, H.R., Khan, M., et al. (2022). Genome-wide CRISPR screen identifies PRC2 and KMT2D-COMPASS as regulators of distinct EMT trajectories that contribute differentially to metastasis. Nat. Cell Biol. *24*, 554–564.

70. Pan, Y., Han, H., Hu, H., Wang, H., Song, Y., Hao, Y., Tong, X., Patel, A.S., Misirlioglu, S., Tang, S., et al. (2023). KMT2D deficiency drives lung squamous cell carcinoma and hypersensitivity to RTK-RAS inhibition. Cancer Cell *41*, 88–105.e8.

71. Doig, K.D., Fellowes, A.P., and Fox, S.B. (2023). Homologous Recombination Repair Deficiency: An Overview for Pathologists. Mod. Pathol. *36*, 100049.

72. Makker, V., Colombo, N., Casado Herráez, A., Santin, A.D., Colomba, E., Miller, D.S., Fujiwara, K., Pignata, S., Baron-Hay, S., Ray-Coquard, I., et al. (2022). Lenvatinib plus Pembrolizumab for Advanced Endometrial Cancer. N. Engl. J. Med. *386*, 437–448.

73. Liu, X., Feng, D., Wang, W., Liang, J., Yu, H., and Ling, B. (2023). Tumor Microenvironment CD8 T and Treg Cells-related Genes Signature Distinguishes Distinct Prognosis and Targeted Therapies Response in Endometrial Cancer. J. Immunother. *46*, 178–191.

74. Zhou, Z., Chen, M.J.M., Luo, Y., Mojumdar, K., Peng, X., Chen, H., Kumar, S.V., Akbani, R., Lu, Y., and Liang, H. (2022). Tumor-intrinsic SIRPA promotes sensitivity to checkpoint inhibition immunotherapy in melanoma. Cancer Cell *40*, 1324–1340.e8.

75. Zhang, Y., Vu, T., Palmer, D.C., Kishton, R.J., Gong, L., Huang, J., Nguyen, T., Chen, Z., Smith, C., Livák, F., et al. (2022). A T cell resilience model associated with response to immunotherapy in multiple tumor types. Nat. Med. *28*, 1421–1431.

76. Ma, X., Dong, L., Liu, X., Ou, K., and Yang, L. (2022). POLE/POLD1 mutation and tumor immunotherapy. J. Exp. Clin. Cancer Res. *41*, 216.

77. Shimasaki, N., Jain, A., and Campana, D. (2020). NK cells for cancer immunotherapy. Nat. Rev. Drug Discov. *19*, 200–218.

78. Elia, I., Rowe, J.H., Johnson, S., Joshi, S., Notarangelo, G., Kurmi, K., Weiss, S., Freeman, G.J., Sharpe, A.H., and Haigis, M.C. (2022). Tumor cells dictate anti-tumor immune responses by altering pyruvate utilization and succinate signaling in CD8(+) T cells. Cell Metabol. *34*, 1137–1150.e6.

79. Chen, D., Zhang, X., Li, Z., and Zhu, B. (2021). Metabolic regulatory crosstalk between tumor microenvironment and tumor-associated macrophages. Theranostics *11*, 1016–1030.

80. Tran, K.A., Kondrashova, O., Bradley, A., Williams, E.D., Pearson, J.V., and Waddell, N. (2021). Deep learning in cancer diagnosis, prognosis and treatment selection. Genome Med. *13*, 152.

81. Yang, W., Soares, J., Greninger, P., Edelman, E.J., Lightfoot, H., Forbes, S., Bindal, N., Beare, D., Smith, J.A., Thompson, I.R., et al. (2013). Genomics of Drug Sensitivity in Cancer (GDSC): a resource for therapeutic biomarker discovery in cancer cells. Nucleic Acids Res. *41*, D955–D961.

82. Iorio, F., Knijnenburg, T.A., Vis, D.J., Bignell, G.R., Menden, M.P., Schubert, M., Aben, N., Gonçalves, E., Barthorpe, S., Lightfoot, H., et al. (2016). A Landscape of Pharmacogenomic Interactions in Cancer. Cell *166*, 740–754.

83. Garnett, M.J., Edelman, E.J., Heidorn, S.J., Greenman, C.D., Dastur, A., Lau, K.W., Greninger, P., Thompson, I.R., Luo, X., Soares, J., et al. (2012). Systematic identification of genomic markers of drug sensitivity in cancer cells. Nature *483*, 570–575.

84. Basu, A., Bodycombe, N.E., Cheah, J.H., Price, E.V., Liu, K., Schaefer, G.I., Ebright, R.Y., Stewart, M.L., Ito, D., Wang, S., et al. (2013). An interactive resource to identify cancer genetic and lineage dependencies targeted by small molecules. Cell *154*, 1151–1161.

85. Seashore-Ludlow, B., Rees, M.G., Cheah, J.H., Cokol, M., Price, E.V., Coletti, M.E., Jones, V., Bodycombe, N.E., Soule, C.K., Gould, J., et al. (2015). Harnessing Connectivity in a Large-Scale Small-Molecule Sensitivity Dataset. Cancer Discov. *5*, 1210–1223.

86. Rees, M.G., Seashore-Ludlow, B., Cheah, J.H., Adams, D.J., Price, E.V., Gill, S., Javaid, S., Coletti, M.E., Jones, V.L., Bodycombe, N.E., et al. (2016). Correlating chemical sensitivity and basal gene expression reveals mechanism of action. Nat. Chem. Biol. *12*, 109–116.

87. Ghandi, M., Huang, F.W., Jané-Valbuena, J., Kryukov, G.V., Lo, C.C., McDonald, E.R., Barretina, J., Gelfand, E.T., Bielski, C.M., Li, H., et al. (2019). Next-generation characterization of the Cancer Cell Line Encyclopedia. Nature *569*, 503–508.

88. Li, H., Ning, S., Ghandi, M., Kryukov, G.V., Gopal, S., Deik, A., Souza, A., Pierce, K., Keskula, P., Hernandez, D., et al. (2019). The landscape of cancer cell line metabolism. Nat. Med. *25*, 850–860.

89. Mak, M.P., Tong, P., Diao, L., Cardnell, R.J., Gibbons, D.L., William, W.N., Skoulidis, F., Parra, E.R., Rodriguez-Canales, J., Wistuba, I.I., et al. (2016). A Patient-Derived, Pan-Cancer EMT Signature Identifies Global Molecular Alterations and Immune Target Enrichment Following Epithelial-to-Mesenchymal TransitionPan-Cancer EMT Molecular and Immune Alterations. Clin. Cancer Res. *22*, 609–620.

90. Timms, K.M., Abkevich, V., Hughes, E., Neff, C., Reid, J., Morris, B., Kalva, S., Potter, J., Tran, T.V., Chen, J., et al. (2014). Association of BRCA1/2 defects with genomic scores predictive of DNA damage repair deficiency among breast cancer subtypes. Breast Cancer Res. *16*, 475.

91. Charoentong, P., Finotello, F., Angelova, M., Mayer, C., Efremova, M., Rieder, D., Hackl, H., and Trajanoski, Z. (2017). Pan-cancer Immunogenomic Analyses Reveal Genotype-Immunophenotype Relationships and Predictors of Response to Checkpoint Blockade. Cell Rep. *18*, 248–262.

92. Jia, Q., Wu, W., Wang, Y., Alexander, P.B., Sun, C., Gong, Z., Cheng, J.N., Sun, H., Guan, Y., Xia, X., et al. (2018). Local mutational diversity drives intratumoral immune heterogeneity in non-small cell lung cancer. Nat. Commun. *9*, 5361.

93. Fu, J., Karen, L., Zhang, W., Jiang, P., and Liu, X. (2019). TIDE-E: an online evaluator of tumor immune-suppressive function of gene sets. Eur. J. Immunol. *49*, 1265–1266.

94. Pang, Z., Chong, J., Zhou, G., de Lima Morais, D.A., Chang, L., Barrette, M., Gauthier, C., Jacques, P.É., Li, S., and Xia, J. (2021). MetaboAnalyst 5.0: narrowing the gap between raw spectra and functional insights. Nucleic Acids Res. *49*, W388–W396.